Chapter 5

Homogenization of elasto-plastic composites

[1] Mean-field homogenization schemes previously developed in the context of linear elasticity are now extended to nonlinear behaviors and firstly to elasto-plasticity. After a brief review of the constitutive equations, these are linearized so that homogenization schemes apply and allow the computation of the effective response.

5.1 Constitutive equations

The J_2 elasto-plastic model described hereafter is presented in Doghri [24] and relies on the von Mises equivalent stress which is the second invariant of the deviatoric stress tensor. In elasto-plasticity, the Hookean law and the additive decomposition of the total strain are given by:

$$\boldsymbol{\sigma} = \boldsymbol{C} : \boldsymbol{\varepsilon}^e, \qquad \boldsymbol{\varepsilon} = \boldsymbol{\varepsilon}^e + \boldsymbol{\varepsilon}^p, \tag{5.1}$$

where $\boldsymbol{C}$ is the Hookean elastic stiffness tensor, $\boldsymbol{\varepsilon}$ is the total strain tensor, $\boldsymbol{\varepsilon}^e$ is the elastic part and $\boldsymbol{\varepsilon}^p$ the plastic one. A yield function f defines an elastic region ($f \leq 0$) and a yield surface ($f = 0$) as:

$$f(\boldsymbol{\sigma}, p) = \sigma_{eq} - \sigma_Y - R(p), \tag{5.2}$$

[1]Some developments of this chapter led to two publications: "A study of various estimates of the macroscopic tangent operator in the incremental homogenization of elasto-plastic composites", Pierard O. and Doghri I., *International Journal for Multiscale Computational Engineering*, accepted for publication [79] and "Micromechanics of elasto-plastic materials reinforced with ellipsoidal inclusions", Pierard O., González C., Segurado J., LLorca J. and Doghri I., *Mechanics of Materials*, submitted for publication [81].

where σ_Y is the initial yield stress and $R(p)$ the hardening function. It is commonly written as a power law function: $R(p) = kp^n$, where k is the hardening modulus and n is the hardening exponent. The plastic flow rule governs the evolution of the plastic strain as:

$$\dot{\boldsymbol{\varepsilon}}^p = \dot{\gamma} \frac{\partial f}{\partial \boldsymbol{\sigma}}, \tag{5.3}$$

where the scalar $\dot{\gamma} \geq 0$ is the plastic multiplier. Its sign is positive if $f = 0$ and $\dot{f} = 0$ (yielding in plasticity) or nil if $f < 0$ (elasticity) or $f = 0$ and $\dot{f} < 0$ (unloading).

The accumulated plasticity p is an internal variable of the model which keeps track of the past history undergone by the material and is linked to the viscoplastic law as:

$$p(t) = \int_0^t \dot{p} d\tau, \qquad \dot{p} = \left(\frac{2}{3} \dot{\boldsymbol{\varepsilon}}^p : \dot{\boldsymbol{\varepsilon}}^p \right)^{1/2} = \dot{\gamma}, \tag{5.4}$$

where $\dot{\boldsymbol{\varepsilon}}^p$ is the plastic strain rate.

5.2 Homogenization of elasto-plastic composites

Homogenization models developed for non-linear composite materials rely on the definition of a linear comparison composite (LCC). This fictitious composite has the same geometry as the original one but the non-linear constitutive laws of its various phases are linearized in such a way that mean-field homogenization schemes valid in linear (thermo-)elasticity apply. The different linearizations lead to various formulations of the local behavior.

First attempt of homogenization for elasto-plastic composites was made by Kröner [54] (and followed in the same time by Budiansky and Wu [16]) who proposed a self-consistent model for polycrystals in which interactions between the phases are only elastic. This led to too stiff responses. Another approach was proposed by Hill [42] who linearized the local constitutive laws written in rate form and introduced an instantaneous elasto-plastic tangent modulus to compute the mechanical response of elasto-plastic materials through a step-by-step iterative procedure. However, when dealing with high non-linearities, predictions become very close to a far upper bound. Berveiller and Zaoui [8] proposed an isotropic interaction law instead of the anisotropic one used by Hill.

Four different formulations are presented here. The secant one relates directly the total strain to the total stress. The version used in this work has been implemented by González and LLorca [37]. The incremental formulation, which will be studied in-depth theoretically and numerically, is written in a rate form. For exhaustiveness purpose, a short introduction is given to the variational formulation which is based on energy concepts and involves an optimization step. However, this formulation is limited to constitutive laws which derive from a single potential. A last linearization, the affine formulation, will be presented in the elasto-viscoplastic section (chapter 6) since we use it only for this class of composites.

For linear homogeneous materials, stiffness and compliance tensors remain uniform within a phase, even if strain and stress fields are not. This is not true anymore with non-linear materials for which instantaneous (secant or tangent) stiffness and compliance tensors are defined at each point of a phase. This fact leads to a crucial problem when solving the homogenization step of the LCC since an infinity of phases is present. One way to circumvent it is to define a reference state for each constituent which enables to have representative moduli of this phase. Generally, the average stress or strain in the phase are considered as the reference state. However, especially when strong gradients occur, such definition of the reference state is not that accurate. Another one based on the second order moment of the stress tensor is presented for the secant formulation in section 5.2.1.

5.2.1 Secant formulation

The secant formulation determines for each phase a secant operator which links the total strain to the total stress. Implementation of the present version is due to González and LLorca [37] for two-phase elasto-plastic material. For a better coherence with subsequent sections, the algorithm described hereafter is written in a strain driven way even if its dual form has been implemented. However, these two approaches are rigorously equivalent (Suquet [95]).

Strains and stresses of an elasto-plastic phase r are related through a secant stiffness tensor $\boldsymbol{C}_r^s$ as:

$$\boldsymbol{\sigma}_r = \boldsymbol{C}_r^s : \boldsymbol{\varepsilon}_r \qquad \text{with} \qquad \boldsymbol{C}_r^s = 3\kappa_r \boldsymbol{I}^{vol} + 2\mu_r^s(\tilde{\boldsymbol{\varepsilon}}_r^{eq})\boldsymbol{I}^{dev}, \tag{5.5}$$

where μ_r^s is the secant shear modulus, which is a function of the per phase reference equivalent strain $\tilde{\boldsymbol{\varepsilon}}_r^{eq}$.

The equivalent macroscopic relation makes use of the effective stiffness tensor $\bar{\boldsymbol{C}}$ as:

$$\bar{\boldsymbol{\sigma}} = \bar{\boldsymbol{C}}(\tilde{\varepsilon}_0^{eq}, \tilde{\varepsilon}_1^{eq}) : \bar{\boldsymbol{\varepsilon}}, \tag{5.6}$$

where $\tilde{\varepsilon}_0^{eq}$ and $\tilde{\varepsilon}_1^{eq}$ are the reference equivalent strains in the matrix and inclusions, respectively. These have to be computed from either the first or the second order moment of the strain tensor in each phase as indicated below.

$\bar{\boldsymbol{C}}$ can be determined assuming any linear homogenization scheme defined by its strain concentration tensor (equation (4.28) for two-phase materials). Homogenization of elasto-plastic composites is thus reduced to solving a set of non-linear algebraic equations in $\tilde{\varepsilon}_0^{eq}$. For each value of the applied strain $\bar{\boldsymbol{\varepsilon}}$, a secant effective stiffness tensor of the composite is determined so that the effective response of the composite can be computed through equation (5.6). From the practical viewpoint, this set is solved using a fixed point algorithm, which begins with a trial value of the secant stiffness tensor of the matrix (the one computed in the previous loading step).

In order to define the reference state of each phase, two methods are proposed. In the classical approach (or first order method), the reference equivalent strain in phase r is determined from the deviatoric part of the average strain tensor $<\boldsymbol{\varepsilon}>_r^{dev}$ of that phase:

$$\tilde{\boldsymbol{\varepsilon}}_r^{eq} = \left[\frac{2}{3} <\boldsymbol{\varepsilon}>_{\omega_r}^{dev} : <\boldsymbol{\varepsilon}>_{\omega_r}^{dev} \right]^{1/2}, \tag{5.7}$$

while in the modified (or second order method) it is computed from the second order moment of the effective strain in the phase as in Ponte Castañeda [83] and Suquet [94]:

$$\tilde{\boldsymbol{\varepsilon}}_r^{eq} = \left[\frac{2}{3} \boldsymbol{I}^{dev} :: <\boldsymbol{\varepsilon} \otimes \boldsymbol{\varepsilon}>_{\omega_r} \right]^{1/2}, \tag{5.8}$$

and an analytical expression of $<\boldsymbol{\varepsilon} \otimes \boldsymbol{\varepsilon}>_{\omega_r}$ was proposed by Buryachenko [17] and given in Suquet [95] for sphere-reinforced composite. This is valid in linear elasticity for a given homogenization scheme. However, when dealing with non linear behaviors, it can be used on the LCC. The extension to ellipsoidal inclusions is done at a higher computational cost and requires the computation of the derivatives of the Eshelby's tensor with respect to the Poisson's ratio (details in Pierard *et al.* [81]).

5.2.2 Incremental formulation

The incremental approach is another option to predict both macroscopic and per-phase responses of non-linear materials. This is done incrementally over several time-steps. The implementation of this formulation is more involved than the secant first-order one but enables to deal with any elasto-plastic model in any phase and a wider range of loading paths (e.g.: non-proportional and cyclic loadings) since it follows the deformation history.

The rate form of the elasto-plastic behavior of phase r reads:

$$\dot{\boldsymbol{\sigma}}_r = \boldsymbol{C}_r^{ep} : \dot{\boldsymbol{\varepsilon}}_r, \tag{5.9}$$

where $\boldsymbol{C}_r^{ep}$ is the so-called continuum elasto-plastic tangent operator. When considering finite time increments for numerical implementation, a discretization in time over each time interval gives:

$$\Delta\boldsymbol{\sigma}_r \approx \boldsymbol{C}_r^{alg} : \Delta\boldsymbol{\varepsilon}_r, \tag{5.10}$$

where $\Delta\boldsymbol{\sigma}_r$ and $\Delta\boldsymbol{\varepsilon}_r$ are stress and strain increments of phase r over the time interval and $\boldsymbol{C}_r^{alg}$ is the algorithmic tangent operator. It is emphasized that the two tangent operators are different in general and become close for vanishingly small plastic strain increments.

Both continuum and consistent tangent operators can be computed analytically for most constitutive models. For the J_2 elasto-plastic model considered in this study, they read:

$$\boldsymbol{C}_r^{alg} = \boldsymbol{C}_r^{ep} - (2\mu_r)^2 \frac{\Delta p_r}{\sigma_r^{eq,tr}} \left(\frac{3}{2} \boldsymbol{I}^{dev} - \boldsymbol{N}_r \otimes \boldsymbol{N}_r \right), \tag{5.11}$$

$$\boldsymbol{C}_r^{ep} = \boldsymbol{C}_r - \frac{(2\mu_r)^2}{3\mu_r + \frac{d\boldsymbol{\sigma}_r^{eq}}{dp_r}} \boldsymbol{N}_r \otimes \boldsymbol{N}_r, \qquad \boldsymbol{N}_r = \frac{3}{2} \frac{\boldsymbol{\sigma}_r^{dev}}{\sigma_r^{eq}}, \tag{5.12}$$

where $\sigma_r^{eq,tr}$ is an elastic predictor of the equivalent stress of phase r at the end of the considered time step and $\boldsymbol{N}_r$ is the normal to the yield surface in stress space of phase r. Both tangent operators are anisotropic during a plastic increment even for isotropic materials.

Equation (5.10-5.12) written for each phase thus define a set of linearized constitutive equations over the time step. Given the state of deformation at the beginning of the time step, homogenization models valid in linear elasticity can apply over this time interval so that the effective relation reads:

$$\Delta\bar{\boldsymbol{\sigma}} = \bar{\boldsymbol{C}}(\tilde{\sigma}_0^{eq}, \tilde{\sigma}_1^{eq}) : \Delta\bar{\boldsymbol{\varepsilon}}, \tag{5.13}$$

where $\bar{\boldsymbol{C}}$ is the macroscopic tangent operator. In this approach, the considered reference equivalent stresses in the phases are computed from the average stress tensor. Extension of the incremental approach by taking into account the second order moment of the stress tensor is still an open subject. Similarly to developments valid for the secant approaches, the effective tangent operator $\bar{\boldsymbol{C}}$ can be evaluated once a homogenization scheme is assumed and is given by (4.28). The strain concentration tensors are the ones used in the context of linear elasticity (section 4.2.3) but their arguments are the elasto-plastic tangent operators in each phase. This set of equations is solved in a strain driven way. Given a macroscopic strain increment over the time step, a trial value of the average strain increment in the inclusions is computed. A fixed point iterative scheme converges to average strain values in the phases from which the effective stiffness and the macroscopic response can be computed. Various results obtained with this formulation are presented in Doghri and Ouaar [26] for spherical reinforcements and in Doghri and Friebel [25] for other inclusion shapes. As presented in section 5.3, various computations of the macroscopic tangent stiffness are possible by considering isotropic or transversely isotropic extraction of the tangent modulus of the matrix.

5.2.3 Variational formulation

Developments presented hereafter follow the review paper of Ponte Castañeda [86], who made the major developments of this formulation. This approach is valid for heterogeneous hyperelastic materials for which, at each point, the local constitutive law derives from a single potential:

$$\boldsymbol{\sigma} = \frac{\partial w}{\partial \boldsymbol{\varepsilon}}(\boldsymbol{\varepsilon}). \tag{5.14}$$

For a strain tensor field $\boldsymbol{\varepsilon}$ within the set of kinematically admissible ones $\mathcal{K}$, the macroscopic stress can be determined from the effective energy function $\bar{\boldsymbol{W}}(\bar{\varepsilon})$ as (Hill [41]):

$$\bar{\boldsymbol{\sigma}} = \frac{\partial \bar{\boldsymbol{W}}}{\partial \bar{\varepsilon}}, \qquad \bar{\boldsymbol{W}}(\bar{\varepsilon}) = \min_{\boldsymbol{\varepsilon}\in\mathcal{K}} \left[(1-v_1) < w_0(\boldsymbol{\varepsilon}) >_{\omega_0} + v_1 < w_1(\boldsymbol{\varepsilon}) >_{\omega_1}\right]. \tag{5.15}$$

A dual form exists and both are exactly equivalent.

Similarly to the other formulations, the effective energy function cannot be determined easily and approximations must be made. The local potential can be approximated by the sum of a Taylor expansion w_r^T of w_r around a reference strain $\tilde{\boldsymbol{\varepsilon}}_r$ and a per phase constant corrector function V_r [2]:

$$\begin{aligned}
w_r(\boldsymbol{\varepsilon}) &\approx w_r^T(\boldsymbol{\varepsilon}) + V_r(\tilde{\boldsymbol{\varepsilon}}_r, \boldsymbol{L}_r^0),\\
w_r^T(\boldsymbol{\varepsilon}) &= w_r(\tilde{\boldsymbol{\varepsilon}}_r) + \frac{\partial w_r}{\partial \boldsymbol{\varepsilon}}(\tilde{\boldsymbol{\varepsilon}}_r) : (\boldsymbol{\varepsilon} - \tilde{\boldsymbol{\varepsilon}}_r) + \frac{1}{2}(\boldsymbol{\varepsilon} - \tilde{\boldsymbol{\varepsilon}_r}) : \boldsymbol{L}_r^0 : (\boldsymbol{\varepsilon} - \tilde{\boldsymbol{\varepsilon}}_r),\\
V_r(\tilde{\boldsymbol{\varepsilon}}_r, \boldsymbol{L}_r^0) &= \underset{\hat{\boldsymbol{\varepsilon}}_r}{stat}\left[w_r(\hat{\boldsymbol{\varepsilon}}_r) - w_r^T(\hat{\boldsymbol{\varepsilon}}_r)\right],
\end{aligned} \tag{5.16}$$

where $\boldsymbol{L}_r^0$ is a uniform modulus tensor and *stat* means optimizing with respect to the relevant variable. A volume average over the composite enables to get an approximation of the effective potential:

$$\begin{aligned}
\bar{W}(\bar{\varepsilon}) &\approx \bar{W}^T(\bar{\varepsilon}; \tilde{\boldsymbol{\varepsilon}}_s, \boldsymbol{L}_s^0) + \sum_{r=1}^{N} v_r V_r(\tilde{\boldsymbol{\varepsilon}}_r, \boldsymbol{L}_r^0),\\
\bar{W}^T(\bar{\varepsilon}, \tilde{\boldsymbol{\varepsilon}}_s, \boldsymbol{L}_s^0) &= \min_{\boldsymbol{\varepsilon}\in\mathcal{K}} < w^T(\boldsymbol{\varepsilon}) >,
\end{aligned} \tag{5.17}$$

where w^T is the volume average of the approximated local potentials w_r^T. An optimization process over the variables $\boldsymbol{\varepsilon}_r$ and $\boldsymbol{L}_r^0$ which depends on the choice of the corrector function enables to derive various estimates and bounds.

A first choice reduces the stationary condition in (5.16) to finding a maximum (Ponte Castañeda [83]) which leads to a linear elastic comparison composite so that a secant effective constitutive relation can be written (deBotton

[2]Such approximation of the potential corresponds to a fictitious linear thermo-elastic material since $\boldsymbol{\sigma}_r(\boldsymbol{\varepsilon}) \approx \frac{\partial w_r}{\partial \boldsymbol{\varepsilon}}(\tilde{\boldsymbol{\varepsilon}}_r) + \boldsymbol{L}_r^0 : (\boldsymbol{\varepsilon} - \tilde{\boldsymbol{\varepsilon}}_r) = \boldsymbol{L}_r^0 : \boldsymbol{\varepsilon} + \left(\frac{\partial w_r}{\partial \boldsymbol{\varepsilon}}(\tilde{\boldsymbol{\varepsilon}}_r) - \boldsymbol{L}_r^0 : \tilde{\boldsymbol{\varepsilon}}_r\right)$.

and Ponte Castañeda [22]). Bounds and estimates can be found for non-linear materials by using the models developed for linear ones on the linear comparison composite. This method takes into account the second-order moment of the fields.

Another approach consists of choosing $\hat{\varepsilon}_r = \tilde{\varepsilon}_r$, which cancels the corrector function V_r in equation (5.16) (Ponte Castañeda [84]). This method makes use of the tangent moduli of the phases and is called accordingly the tangent second-order estimates because it reproduces exactly to the second-order terms of the asymptotic expansions of Suquet and Ponte Castañeda [97]. The optimizing process lead to per phase reference strains $\tilde{\varepsilon}_r$ equal to the average strain in that phase. This method has the drawback of a duality gap (i.e.: the dual formulation does not lead to the same linear comparison composite and thus a different prediction) and cannot provide bounds. The affine formulation (see section 6.3) is a particular case of this formulation.

A recent improvement of this second-order method takes into account the second-order moment of the stress tensor so that its accuracy is much higher when strong heterogeneities of the fields occur (Ponte Castañeda [85]). This method is called the generalized secant one since it leads to intermediate modulus between the tangent and secant ones.

5.3 Computation of the macroscopic tangent operator

In this section, different computations of the macroscopic tangent modulus are examined. These evaluations have a great impact on the final prediction of the incremental formulation. A theoretical study will first determine relations between the different operators thus computed. This will be later analyzed numerically for various composite materials.

5.3.1 Motivation for a stiffness reduction of the macroscopic tangent operator

Predictions of the classical incremental formulation are known to be too stiff and this is illustrated on the following example. Consider a longitudinal uniaxial tension test performed on an elasto-plastic aluminum matrix (E=71.3 GPa, ν=0.3, σ_Y=246.9 MPa, k=133 MPa and m=0.37) reinforced by elastic SiC whiskers (E=485 GPa, ν=0.2, v_1=22 % and Ar=4.1). Experimental results and 3D FE simulations are taken from Levy and Papazian [56]. Results of the incremental formulation implemented as in section 5.2.2 are also reported on figure 5.1 and are effectively very stiff.

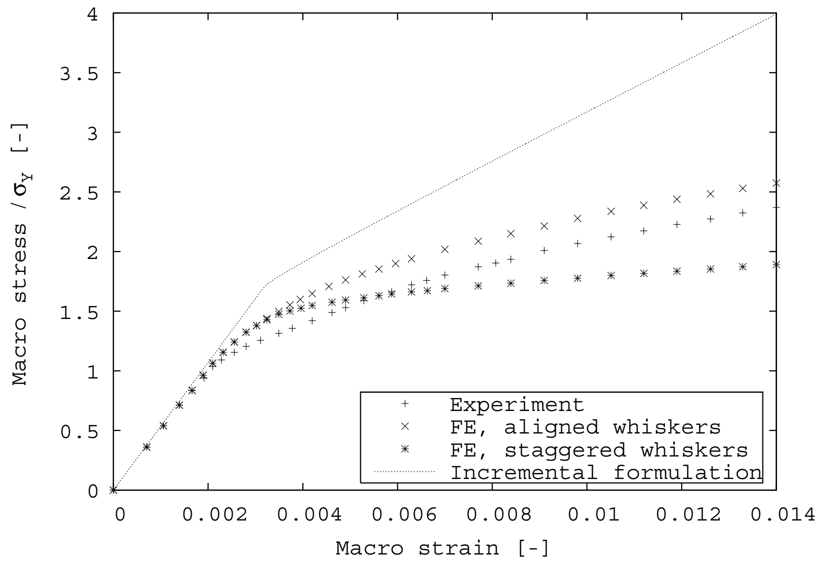

Figure 5.1: Aluminum matrix with SiC whiskers. Longitudinal macroscopic tension test. Illustration of the too stiff response of the incremental formulation.

In the subsequent sections, various attempts to soften the response are presented. The key idea is to consider tensors other than $\boldsymbol{C}_0$ in the computation of the Eshelby, Hill and effective tensors. This can be done by modifying the tensor $\boldsymbol{C}_0$ and extracting its isotropic or transversely isotropic part ($\boldsymbol{C}_0$ is anisotropic during plastic yielding even if the matrix is isotropic). Comparisons between all these tensors are made and their influence on the final response is examined.

5.3.2 Influence of the matrix modulus

A fourth-order tensor $\boldsymbol{C}$ is positive definite (noted $\boldsymbol{C} > 0$) if for all non-nil symmetric second-order tensors $\boldsymbol{\varepsilon}$,

$$\boldsymbol{\varepsilon} : \boldsymbol{C} : \boldsymbol{\varepsilon} > 0. \tag{5.18}$$

By using this quadratic form, two fourth-order tensors can be compared. Notation $\boldsymbol{C} > \boldsymbol{D}$ means that for all non-nil second-order tensors $\boldsymbol{\varepsilon}$, $\boldsymbol{\varepsilon} : \boldsymbol{C} : \boldsymbol{\varepsilon} > \boldsymbol{\varepsilon} : \boldsymbol{D} : \boldsymbol{\varepsilon}$.

An important application of positive definite tensors is when $\boldsymbol{C}$ represents a macroscopic stiffness $\bar{\boldsymbol{C}}$ and $\bar{\boldsymbol{\varepsilon}}$ a strain tensor. If $\bar{\boldsymbol{C}}^{(1)} > \bar{\boldsymbol{C}}^{(2)}$, it means that:

$$\forall\, \bar{\boldsymbol{\varepsilon}} \neq 0,\, \bar{\boldsymbol{\varepsilon}} : \underbrace{\bar{\boldsymbol{C}}^{(1)} : \bar{\boldsymbol{\varepsilon}}}_{\bar{\boldsymbol{\sigma}}^{(1)}} > \bar{\boldsymbol{\varepsilon}} : \underbrace{\bar{\boldsymbol{C}}^{(2)} : \bar{\boldsymbol{\varepsilon}}}_{\bar{\boldsymbol{\sigma}}^{(2)}}. \tag{5.19}$$

So, during a uniaxial test, following relations are guarantee $\bar{\sigma}_{11}^{(1)} > \bar{\sigma}_{11}^{(2)}$ if $\bar{\epsilon}_{11} > 0$ and $\bar{\sigma}_{11}^{(1)} < \bar{\sigma}_{11}^{(2)}$ otherwise.

In this section the dependence of the macroscopic tangent, the Hill's and the Hill's constraint tensors with respect to $\boldsymbol{C}_0$ is analyzed. Our main goal is the following. If $\boldsymbol{C}_0^{(1)} > \boldsymbol{C}_0^{(2)}$, does the relation $\bar{\boldsymbol{C}}^{(1)} > \bar{\boldsymbol{C}}^{(2)}$ hold?

Let $\boldsymbol{C}_0 > 0$ and $\Delta\boldsymbol{C} > 0$. Bornert [10] proved the following relations:

$$\begin{aligned} \boldsymbol{P}(\boldsymbol{C}_0 + \Delta\boldsymbol{C}) &< \boldsymbol{P}(\boldsymbol{C}_0), \\ \boldsymbol{C}^*(\boldsymbol{C}_0) &< \boldsymbol{C}^*(\boldsymbol{C}_0 + \Delta\boldsymbol{C}). \end{aligned} \tag{5.20}$$

Hill's tensor $\boldsymbol{P}$ is thus decreasing with $\boldsymbol{C}_0$ for a given geometry of inclusions on the contrary to Hill's constraint tensor $\boldsymbol{C}^*$ which is an increasing function of $\boldsymbol{C}_0$.

Given a fourth-order tensorial variable $\boldsymbol{A}$, one can prove that the following function f is increasing with $\boldsymbol{A}$ (Bornert [10]):

$$f:\, \boldsymbol{A} \to \left[v_1(\boldsymbol{A} + \boldsymbol{C}_1)^{-1} + (1 - v_1)(\boldsymbol{A} + \boldsymbol{C}_0)^{-1}\right]^{-1} - \boldsymbol{A}. \tag{5.21}$$

Expression (4.27) of the macroscopic tangent operator is form-similar to (5.21). $\bar{\boldsymbol{C}}$ is thus increasing with $\boldsymbol{C}^*$ and therefore with $\boldsymbol{C}_0$:

$$\bar{\boldsymbol{C}}(\boldsymbol{C}_0 + \Delta\boldsymbol{C}) > \bar{\boldsymbol{C}}(\boldsymbol{C}_0),\, \Delta\boldsymbol{C} > 0. \tag{5.22}$$

Furthermore, the dependence of $\bar{\boldsymbol{C}}$ with respect to $\boldsymbol{P}$ is analyzed. By using relations (4.26) and (4.36), the macroscopic tangent operator can be rewritten as:

$$\begin{aligned} \bar{\boldsymbol{C}} &= (v_1\boldsymbol{C}_1 : \boldsymbol{B}^{\boldsymbol{\varepsilon}} + (1 - v_1)\boldsymbol{C}_0) : (v_1\boldsymbol{B}^{\boldsymbol{\varepsilon}} + (1 - v_1)\boldsymbol{I})^{-1} \\ &= \boldsymbol{C}_0 + v_1(\boldsymbol{C}_1 - \boldsymbol{C}_0) : \boldsymbol{B}^{\boldsymbol{\varepsilon}} : (v_1\boldsymbol{B}^{\boldsymbol{\varepsilon}} + (1 - v_1)\boldsymbol{I})^{-1} \\ &= \boldsymbol{C}_0 + v_1(\boldsymbol{C}_1 - \boldsymbol{C}_0) : (v_1\boldsymbol{I} + (1 - v_1)\boldsymbol{B}^{\boldsymbol{\varepsilon}-1})^{-1} \\ &= \boldsymbol{C}_0 + v_1[(\boldsymbol{C}_1 - \boldsymbol{C}_0)^{-1} + (1 - v_1)\boldsymbol{P}]^{-1}. \end{aligned} \tag{5.23}$$

Since $\boldsymbol{P}$ is decreasing with $\boldsymbol{C}_0$ and, if in this last expression, $\boldsymbol{P}$ is computed either with $\boldsymbol{C}_0$ or $\boldsymbol{C}_0 + \Delta\boldsymbol{C}$, and the rest of $\bar{\boldsymbol{C}}$ is computed with $\boldsymbol{C}_0$, the following relation holds:

$$\bar{\boldsymbol{C}}(\boldsymbol{P}(\boldsymbol{C}_0 + \Delta\boldsymbol{C}), \boldsymbol{C}_0) > \bar{\boldsymbol{C}}(\boldsymbol{P}(\boldsymbol{C}_0), \boldsymbol{C}_0), \quad \Delta\boldsymbol{C} > 0. \tag{5.24}$$

5.3.3 Isotropic parts of an anisotropic modulus tensor

Any fourth-order isotropic tensor can always be written under the form (Suquet and Bornert *et al.* [96]):

$$\boldsymbol{C}^{iso} = 3\kappa \boldsymbol{I}^{vol} + 2\mu \boldsymbol{I}^{dev} = (\boldsymbol{I}^{vol} :: \boldsymbol{C}^{iso})\boldsymbol{I}^{vol} + \frac{1}{5}(\boldsymbol{I}^{dev} :: \boldsymbol{C}^{iso})\boldsymbol{I}^{dev}, \quad (5.25)$$

where κ and μ are the bulk and shear moduli, respectively, $\boldsymbol{I}^{vol} = \frac{1}{3}\mathbf{1} \otimes \mathbf{1}$ and $\boldsymbol{I}^{dev} = \boldsymbol{I} - \boldsymbol{I}^{vol}$ are the spherical and deviatoric operators, respectively, $\mathbf{1}$ is the second-order identity tensor and $'::'$ is a tensor product contracted over four indices.

Extracting an isotropic part $\boldsymbol{C}^{iso}$ from an anisotropic modulus tensor $\boldsymbol{C}^{ani}$ consists in finding two scalars κ_t and μ_t so that the isotropic tensor is written as:

$$\boldsymbol{C}^{iso} = 3\kappa_t \boldsymbol{I}^{vol} + 2\mu_t \boldsymbol{I}^{dev}. \quad (5.26)$$

Two extraction methods are proposed hereafter: a general one valid for any anisotropic tensor and a special one.

General method This method proposed by Bornert [11] consists of a projection of the anisotropic tangent operator $\boldsymbol{C}^{ani}$ onto the subspace of isotropic ones so that we get:

$$3\kappa_t = \boldsymbol{I}^{vol} :: \boldsymbol{C}^{ani}, \qquad 10\mu_t = \boldsymbol{I}^{dev} :: \boldsymbol{C}^{ani}. \quad (5.27)$$

In all the simulations, the J_2 elasto-plastic model is used. It is thus interesting to apply this projection method in this particular case. An application of equation (5.27) to $\boldsymbol{C}^{alg}$ gives an isotropic projection $\boldsymbol{C}^{IsoGen}$ defined by

$$\kappa_t = \kappa, \qquad \mu_t = \mu - \frac{3}{5}\mu^2 \left(\frac{1}{h} + 4\frac{\Delta p}{\sigma_{eq}^{tr}}\right). \quad (5.28)$$

Special method Another method was proposed by Ponte Castañeda [84]. It is applicable when the anisotropic tangent operator can be cast under the form:

$$\boldsymbol{C}^{ani} = 3k_1 \boldsymbol{I}^{vol} + 2k_2(\boldsymbol{I}^{dev} - \frac{2}{3}\boldsymbol{N} \otimes \boldsymbol{N}) + 2k_3 \left(\frac{2}{3}\boldsymbol{N} \otimes \boldsymbol{N}\right), \quad (5.29)$$

with $N_{ii} = 0$ and $\boldsymbol{N} : \boldsymbol{N} = \frac{3}{2}$. The method is based on the following fundamental assumption:

$$\text{dev}(\dot{\boldsymbol{\varepsilon}}) // \boldsymbol{N}, \quad (5.30)$$

where $'//'$ means 'is collinear with'. It then follows that:

$$\dot{\boldsymbol{\sigma}} = \boldsymbol{C}^{ani} : \dot{\boldsymbol{\varepsilon}} = \boldsymbol{C}^{IsoSpe} : \dot{\boldsymbol{\varepsilon}}, \quad (5.31)$$

where $\boldsymbol{C}^{IsoSpe}$ is a special isotropic operator defined by:

$$\kappa_t = k_1, \;\; \mu_t = k_3. \tag{5.32}$$

Chaboche *et al.* [18, 19] made the interesting observation that the special isotropic extraction corresponds to a stiffness reduction of $\boldsymbol{C}^{ani}$ in a direction orthogonal to $\boldsymbol{N}$. Indeed, since $(\boldsymbol{I}^{dev} - \frac{2}{3}\boldsymbol{N} \otimes \boldsymbol{N}) : \boldsymbol{N} = \boldsymbol{0}$, and using (5.30), we have:

$$\dot{\boldsymbol{\sigma}} = \boldsymbol{C}^{ani} : \dot{\boldsymbol{\varepsilon}} = \left[\boldsymbol{C}^{ani} + \alpha(\boldsymbol{I}^{dev} - \frac{2}{3}\boldsymbol{N} \otimes \boldsymbol{N})\right] : \dot{\boldsymbol{\varepsilon}} = \boldsymbol{C}^{IsoSpe} : \dot{\boldsymbol{\varepsilon}}. \tag{5.33}$$

With the conditions $2k_3 - 2k_2 - \alpha = 0$ and $2\mu_t = 2k_2 + \alpha$, we do retrieve $\mu_t = k_3$.

For J_2 elasto-plastic model, both anisotropic tangent operators follow equation (5.29) and assumption (5.30) is always valid if $\dot{\boldsymbol{N}} = \boldsymbol{0}$. An application of equation (5.32) gives:

$$\kappa_t = \kappa, \;\; \mu_t = \mu\left(1 - \frac{3\mu}{h}\right). \tag{5.34}$$

Chaboche *et al.* [18, 19] also note that μ_t thus obtained is softer than with the general projection when $\boldsymbol{C}^{ep}$ is considered. We generalize this observation and prove that $\boldsymbol{C}^{IsoGen}$ is stiffer than $\boldsymbol{C}^{IsoSpe}$ for both $\boldsymbol{C}^{ep}$ and $\boldsymbol{C}^{alg}$:

$$\boldsymbol{C}^{IsoGen} - \boldsymbol{C}^{IsoSpe} = \frac{12\mu^2}{5}\left(\frac{1}{h} - \frac{\Delta p}{\sigma_{eq}^{tr}}\right)\boldsymbol{I}^{dev} > 0, \tag{5.35}$$

the scalar factor between brackets being positive (Doghri and Ouaar [26]).

5.3.4 Transversely isotropic parts of an anisotropic modulus tensor

Similarly to the general method for isotropic extraction, a projection is proposed for extracting the transversely isotropic part of an anisotropic fourth-order tensor. The method presented here was first proposed by Walpole [103] and described in Frederico *et al.* [31].

Any transversely isotropic second-order tensor $\boldsymbol{c}$ can be written as a combination of two basis tensors $\boldsymbol{a}$ and $\boldsymbol{b}$:

$$\boldsymbol{c} = c^a\boldsymbol{a} + c^b\boldsymbol{b}, \tag{5.36}$$

where:

$$\boldsymbol{a} = \boldsymbol{w} \otimes \boldsymbol{w}, \;\; \boldsymbol{b} = \boldsymbol{1} - \boldsymbol{a},$$

$\boldsymbol{w}$ being the direction of anisotropy. Any fourth-order transversely isotropic tensor $\boldsymbol{T}$ with a direction of anisotropy $\boldsymbol{w}$ can be written as (Bornert [10]):

$$\begin{aligned} \boldsymbol{T} &= (\boldsymbol{B}_1 :: \boldsymbol{T})\boldsymbol{B}_1 + (\boldsymbol{B}_2 :: \boldsymbol{T})\boldsymbol{B}_2 + \frac{1}{2}(\boldsymbol{B}_3 :: \boldsymbol{T})\boldsymbol{B}_3 \\ &\quad + \frac{1}{2}(\boldsymbol{B}_4 :: \boldsymbol{T})\boldsymbol{B}_4 + \frac{1}{2}(\boldsymbol{B}_5 :: \boldsymbol{T})\boldsymbol{B}_6 + \frac{1}{2}(\boldsymbol{B}_6 :: \boldsymbol{T})\boldsymbol{B}_5, \quad (5.37) \end{aligned}$$

where the six fourth-order basis tensors $\boldsymbol{B}_i$ are constructed as follows:

$$\begin{aligned} (B_1)_{ijkl} &= \frac{1}{2} b_{ij} b_{kl}, \quad (5.38) \\ (B_2)_{ijkl} &= a_{ij} a_{kl}, \\ (B_3)_{ijkl} &= \frac{1}{2}(b_{ik} b_{jl} + b_{jk} b_{il} - b_{ij} b_{kl}), \\ (B_4)_{ijkl} &= \frac{1}{2}(b_{ik} a_{jl} + b_{il} a_{jk} + b_{jl} a_{ik} + b_{jk} a_{il}), \\ (B_5)_{ijkl} &= a_{ij} b_{kl}, \\ (B_6)_{ijkl} &= b_{ij} a_{kl}. \quad (5.39) \end{aligned}$$

The first four tensors have minor and major symmetries while the last two ones have only the minor symmetries. One can notice that if $T_5 = T_6$ ($T_i = \boldsymbol{B}_i :: \boldsymbol{T}$), the tensor $\boldsymbol{T}$ is fully symmetric ($B_{5ijkl} = B_{6klij}$). In this particular case, the problem is reduced to finding five independent components as expected in the case of transversely isotropic modulus operators. If the first four components T_i are positive, then the tensor $\boldsymbol{T}$ is positive definite.

Let's now consider an arbitrary anisotropic fourth-order tensor $\boldsymbol{C}^{ani}$ which has the minor symmetries. In this case, application of the double contractions in (5.37) on $\boldsymbol{C}^{ani}$ instead of $\boldsymbol{T}$ give the projection of $\boldsymbol{C}^{ani}$ onto the subspace generated by $\boldsymbol{B}_i$, to obtain a transversely isotropic tensor with a direction of anisotropy $\boldsymbol{w}$:

$$\begin{aligned} \boldsymbol{C}^{TrIso} &= (\boldsymbol{B}_1 :: \boldsymbol{C}^{ani})\boldsymbol{B}_1 + (\boldsymbol{B}_2 :: \boldsymbol{C}^{ani})\boldsymbol{B}_2 + \frac{1}{2}(\boldsymbol{B}_3 :: \boldsymbol{C}^{ani})\boldsymbol{B}_3 \quad (5.40) \\ &\quad + \frac{1}{2}(\boldsymbol{B}_4 :: \boldsymbol{C}^{ani})\boldsymbol{B}_4 + \frac{1}{2}(\boldsymbol{B}_5 :: \boldsymbol{C}^{ani})\boldsymbol{B}_6 + \frac{1}{2}(\boldsymbol{B}_6 :: \boldsymbol{C}^{ani})\boldsymbol{B}_5 \end{aligned}$$

Application of this method to the tangent operator $\boldsymbol{C}^{ep}$ (equation (5.12)) of the J_2 elasto-plastic model gives (direction of anisotropy is along axis 1 and

$T_i = \boldsymbol{B}_i :: \boldsymbol{C}^{ani}$):

$$\begin{aligned}
T_1 &= 2\kappa + \frac{2}{3}\mu - \frac{1}{2}(N_{22}^2 + N_{33}^2 + 2N_{22}N_{33})\frac{(2\mu)^2}{h}, \\
T_2 &= \kappa + \frac{4}{3}\mu - N_{11}^2\frac{(2\mu)^2}{h}, \\
T_3 &= 2\mu - \frac{1}{4}(N_{22}^2 + N_{33}^2 - 2N_{22}N_{33} + 2N_{23}^2)\frac{(2\mu)^2}{h}, \\
T_4 &= 2\mu - \frac{1}{2}(2N_{12}^2 + 2N_{13}^2)\frac{(2\mu)^2}{h}, \\
T_5 &= \kappa - \frac{2}{3}\mu - \frac{1}{2}(N_{11}N_{22} + N_{11}N_{33})\frac{(2\mu)^2}{h}, \\
T_6 &= T_5, \qquad (5.41)
\end{aligned}$$

where $h = 3\mu + \frac{d\sigma^{eq}}{dp}$. With these notations, engineering moduli are given by:

$$E_L = T_2 - \frac{T_5^2}{2T_1}, \qquad (5.42)$$

$$\nu_{LT} = \frac{T_5}{2T_1}, \qquad \nu_T = \frac{T_5^2 - (2T_1 - T_3)T_2}{T_6^2 - (2T_1 + T_3)T_2}, \qquad (5.43)$$

$$\mu_{LT} = \frac{T_3}{4}, \qquad \mu_T = \frac{T_4}{4}, \qquad (5.44)$$

where E_L is the Young's modulus in the longitudinal direction (the one of anisotropy), ν_{LT} is the Poisson's ratio for a traction test in the longitudinal direction, ν_T is the Poisson's ratio in the transverse plane, μ_{LT} is the shear modulus along the longitudinal direction and μ_T is the shear modulus in the transverse plane.

For the J_2 elasto-plastic model under monotonic loading, assumption (5.30) is verified and therefore equation (5.31) always holds and gives an isotropic tangent operator. Nevertheless, based on the fact that the special method for extracting the isotropic part of a tensor gives a softer tangent, we propose the following more compliant approximation of the anisotropic tangent:

$$\boldsymbol{C}^{AniSpe} = \boldsymbol{C}^{ani} - K\frac{(2\mu)^2}{h}\boldsymbol{N} \otimes \boldsymbol{N}, \qquad (5.45)$$

where $K > 1$ is a softening factor. Applying the general transversely isotropic extraction on this modified tensor will give a new transversely isotropic tensor. This approach will be called the special transversely isotropic method. The particular case of $K = 1$ (no softening added) is called the general transversely isotropic method.

5.3.5 Comparison of various local tangent operators

In this section, the various local tangent operators of the J_2 plasticity model are compared in the meaning of the quadratic forms. Doghri and Ouaar [26] already proved that

$$\boldsymbol{C}^{ep} \geq \boldsymbol{C}^{alg} \geq \boldsymbol{C}^{IsoSpe}. \tag{5.46}$$

Our next goal is to find similar relations involving $\boldsymbol{C}^{IsoGen}$. The results hereafter hold for both $\boldsymbol{C}^{alg}$ ($\Delta p > 0$) and $\boldsymbol{C}^{ep}$ (by setting $\Delta p \to 0$) so that the anisotropic tangent operator is denoted $\boldsymbol{C}^{ani}$. Results of section 5.3.3 give:

$$\boldsymbol{C}^{IsoGen} - \boldsymbol{C}^{ani} = -H\left[\boldsymbol{I}^{dev} - \frac{10}{3}\boldsymbol{N}\otimes\boldsymbol{N}\right], \quad H = \frac{6}{5}\mu^2\left(\frac{1}{h} - \frac{\Delta p}{\sigma_{eq}^{tr}}\right) > 0. \tag{5.47}$$

The proof for $H > 0$ is given in Doghri and Ouaar [26]. Unfortunately, the tensor might be not positive definite. However, some interesting relations are found in the following case:

$$\boldsymbol{\sigma} = \begin{bmatrix} a & b & b & 0 & 0 & 0 \end{bmatrix}^T, \tag{5.48}$$

where the scalars a and b are of opposite signs. Under these conditions and if fourth-order tensors are stored under the usual engineering way, following result is obtained:

$$\boldsymbol{C}^{IsoGen} - \boldsymbol{C}^{ani} = H\begin{pmatrix} 8/3 & -4/3 & -4/3 & 0 & 0 & 0 \\ -4/3 & 1/6 & 7/6 & 0 & 0 & 0 \\ -4/3 & 7/6 & 1/6 & 0 & 0 & 0 \\ 0 & 0 & 0 & -1 & 0 & 0 \\ 0 & 0 & 0 & 0 & -1 & 0 \\ 0 & 0 & 0 & 0 & 0 & -1 \end{pmatrix}. \tag{5.49}$$

For stresses given by equation (5.48), the strains have the following form:

$$\boldsymbol{\varepsilon} = \begin{bmatrix} \varepsilon_{11} & \varepsilon_{22} & \varepsilon_{33} & 0 & 0 & 0 \end{bmatrix}^T, \tag{5.50}$$

where $sign(\varepsilon_{11}) = sign(a)$; $sign(\varepsilon_{22}) = sign(\varepsilon_{33}) = -sign(a)$. For these strains, we obtain:

$$\begin{aligned} \boldsymbol{\varepsilon} : (\boldsymbol{C}^{IsoGen} - \boldsymbol{C}^{ani}) : \boldsymbol{\varepsilon} \quad = \quad & H\Big(\frac{8}{3}\boldsymbol{\varepsilon}_{11}^2 + \frac{1}{6}\boldsymbol{\varepsilon}_{22}^2 + \frac{1}{6}\boldsymbol{\varepsilon}_{33}^2 - \frac{8}{3}\boldsymbol{\varepsilon}_{11}\boldsymbol{\varepsilon}_{22} \\ & + \frac{7}{3}\boldsymbol{\varepsilon}_{22}\boldsymbol{\varepsilon}_{33} - \frac{8}{3}\boldsymbol{\varepsilon}_{11}\boldsymbol{\varepsilon}_{33}\Big) > 0. \end{aligned} \tag{5.51}$$

In this particular case, following relation holds:

$$\boldsymbol{C}^{IsoGen} > \boldsymbol{C}^{ani}, \;\; \boldsymbol{C}^{ani} = \boldsymbol{C}^{ep} \;\text{ or }\; \boldsymbol{C}^{alg}. \tag{5.52}$$

It is rather surprising and unexpected to find that $\boldsymbol{C}^{IsoGen}$ is stiffer than $\boldsymbol{C}^{ani}$. Given the form of the stress tensor (5.48), this result is valid for each plastic phase of the composite if a macroscopic tension test is applied. The particular case $b = 0$ corresponds to uniaxial tension in a phase.

5.3.6 Various estimates of the macroscopic tangent operator

Hill's tensor ($\boldsymbol{P}$), the strain concentration tensor ($\boldsymbol{B}^{\boldsymbol{\varepsilon}}$) and the macroscopic tangent operator ($\bar{\boldsymbol{C}}$) make use of $\boldsymbol{C}_0$ as indicated in section 4.2.1 for Mori-Tanaka homogenization scheme. In order to extend the latter model to elasto-plasticity, tangent operators $\boldsymbol{C}_r(t)$ which are homogeneous per phase and defined at a reference equivalent stress $\tilde{\sigma}^{eq}$ are needed:

$$\dot{\boldsymbol{\sigma}}(\boldsymbol{x},t) = \boldsymbol{C}_r(t,\tilde{\sigma}^{eq}) : \dot{\boldsymbol{\varepsilon}}(\boldsymbol{x},t), \quad \forall \boldsymbol{x} \in \omega_r. \tag{5.53}$$

For simplicity, subsequent developments focus on the matrix phase and assume that it obeys J_2 elasto-plastic model. A reference tangent operator $\boldsymbol{C}_0^{ani}(t)$ is computed by sending average matrix strain and strain increments to the J_2 elasto-plastic model. If all computations are made with $\boldsymbol{C}_0^{ani}$ which is anisotropic, this is known to lead to too stiff predictions (see section 5.1). Variations may include evaluation of Eshelby's tensor $\mathcal{E}$, Hill's tensor $\boldsymbol{P}$ or all the macroscopic operator $\bar{\boldsymbol{C}}$ with different approximations of $\boldsymbol{C}_0^{ani}$. In the previous sections, the following instantaneous matrix operators have been defined:

1. Anisotropic operators $\boldsymbol{C}_0^{ani}$, either "continuum" ($\boldsymbol{C}_0^{ep}$, equation (5.12)) or "algorithmic" ($\boldsymbol{C}_0^{alg}$, equation (5.11)).
2. Isotropic part $\boldsymbol{C}_0^{IsoGen}$ using a general projection method - equation (5.27).
3. Isotropic part $\boldsymbol{C}_0^{IsoSpe}$ using a special method - equation (5.32).
4. Transversely isotropic part $\boldsymbol{C}_0^{TrIsoGen}$ using a general projection method (obtained by setting $\boldsymbol{C}^{ani} = \boldsymbol{C}_0^{ep}$ in equation (5.40)).
5. Transversely isotropic part $\boldsymbol{C}_0^{TrIsoSpe}$ using a special method (obtained by computing $\boldsymbol{C}_0^{AniSpe}$ from equation (5.45) and setting $\boldsymbol{C}^{ani} = \boldsymbol{C}_0^{AniSpe}$ in equation (5.40)).

For the computation of various estimates of the macroscopic tangent, the following procedure is proposed.

$$\boldsymbol{P} = \mathcal{E}(\boldsymbol{E}_0) : \boldsymbol{D}_0^{-1}, \tag{5.54}$$

$$\boldsymbol{B}^{\boldsymbol{\varepsilon}} = [\boldsymbol{I} + \boldsymbol{P} : (\boldsymbol{C}_1 - \boldsymbol{C}_0)]^{-1}, \tag{5.55}$$

$$\bar{\boldsymbol{C}} = (v_1 \boldsymbol{C}_1 : \boldsymbol{B}^{\boldsymbol{\varepsilon}} + (1-v_1)\boldsymbol{C}_0) : (v_1 \boldsymbol{B}^{\boldsymbol{\varepsilon}} + (1-v_1)\boldsymbol{I})^{-1}. \tag{5.56}$$

$\boldsymbol{C}_0$, $\boldsymbol{D}_0$ and $\boldsymbol{E}_0$ are various instantaneous operators for the reference matrix discussed above. The classical (but too stiff) case corresponds to the following choice:

$$\boldsymbol{E}_0 = \boldsymbol{D}_0 = \boldsymbol{C}_0 = \boldsymbol{C}_0^{ani} = \boldsymbol{C}_0^{ep}. \tag{5.57}$$

Softer and better predictions were obtained by Doghri and Ouaar [26] and Doghri and Friebel [25] by taking:

$$\boldsymbol{E}_0 = \boldsymbol{C}_0^{IsoGen} \text{ or } \boldsymbol{C}_0^{IsoSpe}; \, \boldsymbol{D}_0 = \boldsymbol{C}_0 = \boldsymbol{C}_0^{ani} = \boldsymbol{C}_0^{alg}. \tag{5.58}$$

Chaboche *et al.* [18, 19] obtained good predictions with the following case:

$$\boldsymbol{E}_0 = \boldsymbol{D}_0 = \boldsymbol{C}_0^{IsoSpe}; \, \boldsymbol{C}_0 = \boldsymbol{C}_0^{ani} = \boldsymbol{C}_0^{ep}. \tag{5.59}$$

Several other variants will be tested in the numerical section.

Notice that evaluation of the Eshelby's tensor is analytical only if $\boldsymbol{E}_0$ is isotropic or transversely isotropic with the restriction that the direction of anisotropy is aligned with the direction of the reinforcements. Expressions in these two cases are different and presented in appendix A. In all other cases, a numerical evaluation is required (Gavazzi and Lagoudas [34]).

5.4 Numerical simulations

5.4.1 Effect of the macroscopic tangent operator's computation

Throughout this section, comparisons are made between the different predictions obtained with various versions of the macroscopic tangent operator of the incremental formulation. Table 5.1 explains which operator is used to compute Eshelby's tensor, Hill's tensor and finally the macroscopic tangent operator.

For all the simulations, the J_2 plasticity model is used and notations of the corresponding parameters were presented in section 5.1. Inclusion's shape is described by the aspect ratio Ar. Subscript 0 refers to the matrix and 1 to the inclusions.

Aluminum matrix with SiC whiskers

Example of section 5.3.1 is picked up again. Confrontation of reference results with different evaluations of Hill's tensor $\boldsymbol{P}$ is reported on figure 5.2a. The extracting method to get the isotropic part of $\boldsymbol{C}_0$ has a considerable impact on the macroscopic prediction. In this case, the special method (*P IsoSpe*) gives acceptable results, the general one being much too stiff (*P IsoGen*). This fact has already been reported by Chaboche *et al.* [19]. Logically, in this test, computing $\boldsymbol{P}$ with the transversely isotropic part or the anisotropic version gives almost the same results, which are both too stiff.

Predictions obtained with a macroscopic tangent operator computed entirely from the same tangent operator of the matrix are reported on figure

Case	Notations	$\boldsymbol{E}_0$ (for $\mathcal{E}$ in eq.(5.54))	$\boldsymbol{D}_0$ (for $\boldsymbol{P}$ in eq. (5.54))	$\boldsymbol{C}_0$ (for $\bar{\boldsymbol{C}}$ in eqs. (5.55-5.56))
1	Esh IsoGen	$\boldsymbol{C}_0^{IsoGen}$	$\boldsymbol{C}_0^{ani}$	$\boldsymbol{C}_0^{ani}$
2	Esh IsoSpe	$\boldsymbol{C}_0^{IsoSpe}$	$\boldsymbol{C}_0^{ani}$	$\boldsymbol{C}_0^{ani}$
3	P IsoGen	$\boldsymbol{C}_0^{IsoGen}$	$\boldsymbol{C}_0^{IsoGen}$	$\boldsymbol{C}_0^{ani}$
4	P IsoSpe	$\boldsymbol{C}_0^{IsoSpe}$	$\boldsymbol{C}_0^{IsoSpe}$	$\boldsymbol{C}_0^{ani}$
5	P TrIsoGen	$\boldsymbol{C}_0^{TrIsoGen}$	$\boldsymbol{C}_0^{TrIsoGen}$	$\boldsymbol{C}_0^{ani}$
6	P TrIsoSpe	$\boldsymbol{C}_0^{TrIsoSpe}$	$\boldsymbol{C}_0^{TrIsoSpe}$	$\boldsymbol{C}_0^{ani}$
7	all IsoGen	$\boldsymbol{C}_0^{IsoGen}$	$\boldsymbol{C}_0^{IsoGen}$	$\boldsymbol{C}_0^{IsoGen}$
8	all IsoSpe	$\boldsymbol{C}_0^{IsoSpe}$	$\boldsymbol{C}_0^{IsoSpe}$	$\boldsymbol{C}_0^{IsoSpe}$
9	all TrIsoGen	$\boldsymbol{C}_0^{TrIsoGen}$	$\boldsymbol{C}_0^{TrIsoGen}$	$\boldsymbol{C}_0^{TrIsoGen}$
10	all Ani	$\boldsymbol{C}_0^{ani}$	$\boldsymbol{C}_0^{ani}$	$\boldsymbol{C}_0^{ani}$

Table 5.1: Notations for the various computations of the macroscopic tangent operator.

5.2b. In this case only the predictions obtained with the special isotropic tangent operator give realistic results. The three other predictions are too stiff, especially with the general isotropic operator !

One can note that it is has been proven that $\bar{\boldsymbol{C}}$ is a monotonic function of the tangent operator of the matrix used for the computation of $\boldsymbol{P}$ (see equation (5.24)), which is well in accordance with figure 5.2a. On the other hand, $\bar{\boldsymbol{C}}$ is also a monotonic function of $\boldsymbol{C}_0$ if $\boldsymbol{E}_0 = \boldsymbol{D}_0 = \boldsymbol{C}_0$, as observed on figure 5.2b. Finally, figure 5.2a shows that *Esh IsoGen* and *Esh IsoSpe* give almost the same results. This is almost always observed and is due to the property of homogeneity of degree zero of $\mathcal{E}$ with respect to $\boldsymbol{C}_0$ (Suquet and Bornert [96]).

Aluminum alloy matrix with long stiff aluminum fibers

Once again, a ductile aluminum alloy matrix (E=68.9 GPa, ν=0.32, σ_Y=94 MPa, k=578.25 MPa and m=0.53) reinforced this time by long stiff alumna fibers (E=344.5 GPa, ν=0.26, v_1=55 % and Ar=1000) is considered.

Figure 5.3 illustrates the various predictions in a longitudinal macroscopic tension test and are compared to 2D FE simulations with an hexagonal arrangement of fibers (Jansson [45]). All the predictions which compute $\boldsymbol{P}$ with different matrix operators ($\boldsymbol{E}_0 \neq \boldsymbol{D}_0$) give non physical results. In fact, this inconsistency gives a non symmetric $\boldsymbol{P}$, which is unacceptable (see section 4.2.1). The overall stiffness is not symmetric either and the transverse response in terms of strains and stresses was found to lose its symmetry.

However, all other predictions (with $\boldsymbol{E}_0 = \boldsymbol{D}_0$) give almost the same results

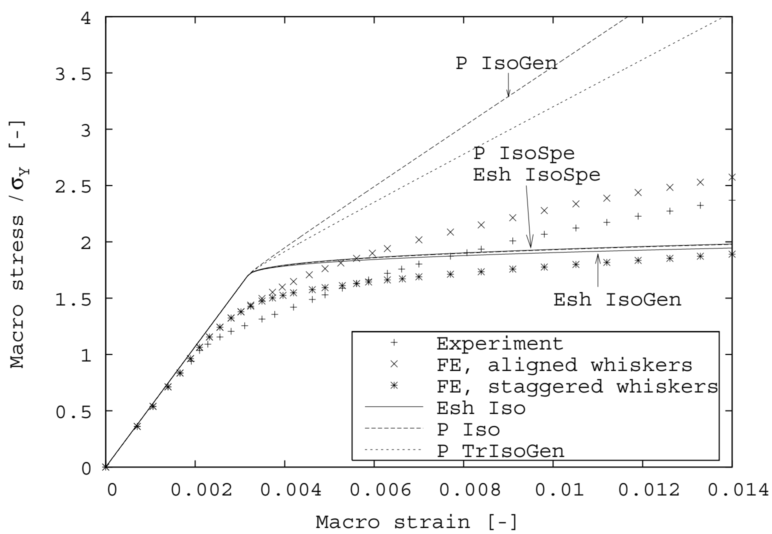

(a) Various computations of $\boldsymbol{P}$.

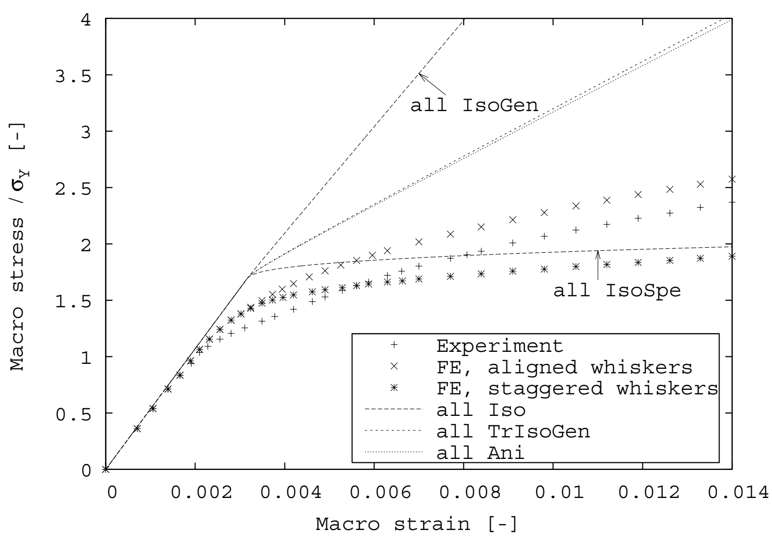

(b) Various computations of $\bar{\boldsymbol{C}}$.

Figure 5.2: Aluminum matrix with SiC whiskers. Longitudinal macroscopic tension test.

as the finite element simulations, excepted *all IsoGen* which is a little bit too

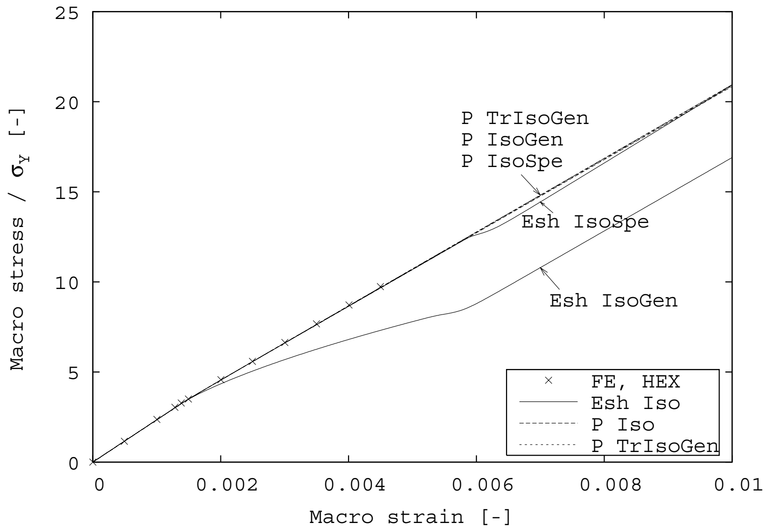

(a) Various computations of $\boldsymbol{P}$.

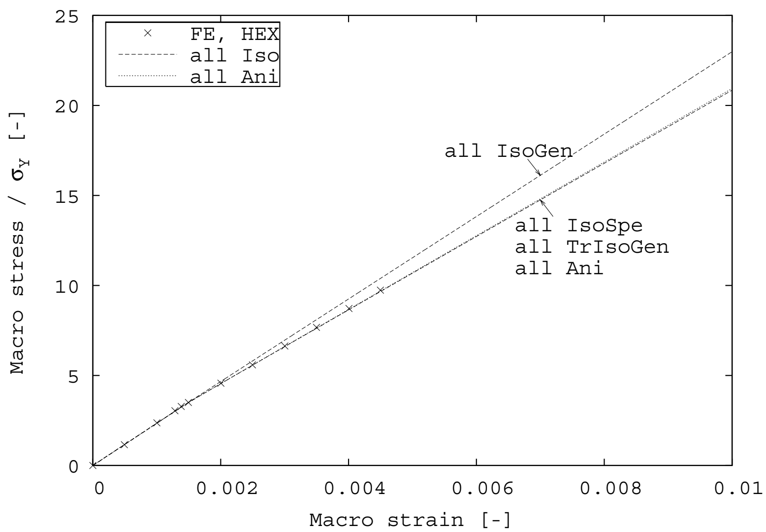

(b) Various computations of $\bar{\boldsymbol{C}}$.

Figure 5.3: Aluminum alloy matrix with long stiff aluminum fibers. Longitudinal macroscopic tension test.

stiff.

Aluminum matrix with fibers

In this simulation, an aluminum alloy matrix (E=70 GPa, ν=0.33, σ_Y=200 MPa, k=2000 MPa and m=1) is reinforced with $\delta-Al_2O_3$ fibers (E=300 GPa, ν=0.2, v_1=10 % and Ar=20). The behavior of such a material was simulated with FE by Kang and Gao [49]. In a tension test in the longitudinal direction, figures 5.4a and 5.4b illustrate the predictions obtained with different evaluations of $\boldsymbol{P}$ and $\bar{\boldsymbol{C}}$, respectively. Note that even if *Esh IsoGen* gives the smallest error, the hardening rate is not predicted accurately so that the most accurate predictions are obtained when making use of the special isotropisation technique. The general transversely isotropic and anisotropic predictions are almost superposed and also too stiff. However, making use of the special transversely isotropic extraction -equations (5.40) and (5.45)- such as illustrated on figure 5.5 softens the response and can even give the best predictions with a relatively small value of the softening coefficient K.

Predictions for a tension test in the transverse direction are reported on figures 5.6a and 5.6b. Interpretation given for the longitudinal case remains valid except that *all TrIsoGen* is much stiffer than *all Ani*. The last one being quite close to the reference solution. Again, with a well chosen value of the softening coefficient, one can get very reliable predictions (see figure 5.7). This is even lower than for longitudinal traction.

MMC under cyclic strain

Different predictions of a metal matrix composite (MMC) (matrix: E=75 GPa, ν=0.30, σ_Y=75 MPa, k=416 MPa and m=0.39; inclusions: E=400 GPa, ν=0.20, v_1=30 % and Ar=1) under cyclic strain are illustrated on figure 5.8 and compared to FE predictions (2D axisymmetric unit cell) of Doghri and Ouaar [26]. Once again this test shows large differences between the different evaluations of the macroscopic tangent operator. Only *Esh Iso* (general and special), *P IsoSpe* and *all IsoSpe* give acceptable results. But once use of the general isotropic extraction of $\boldsymbol{C}_0$ or the anisotropic tangent operator is made in $\boldsymbol{P}$ or $\bar{\boldsymbol{C}}$, results are much stiffer.

MMC under transverse shear

The response of the same MMC (but with 15% of long fibers) undergoing a transverse shear test is confronted to 2D plane strain FE simulations and illustrated on figure 5.9a. As in tensile tests, predictions which make use of the general isotropic extraction (excepted *Esh IsoGen*) or only the anisotropic tangent operator are too stiff while the special methods give much more realistic results. Several predictions with the transversely isotropic extraction are illustrated on figure 5.9b. The too stiff general transversely isotropic prediction can

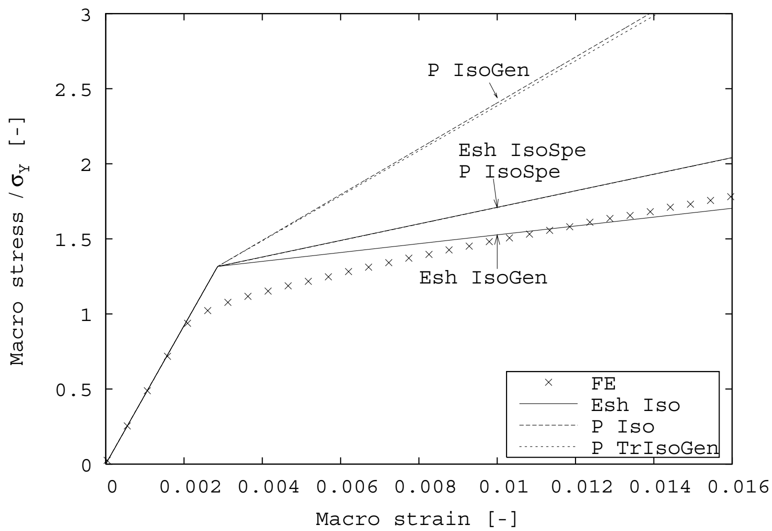

(a) Various computations of $\boldsymbol{P}$.

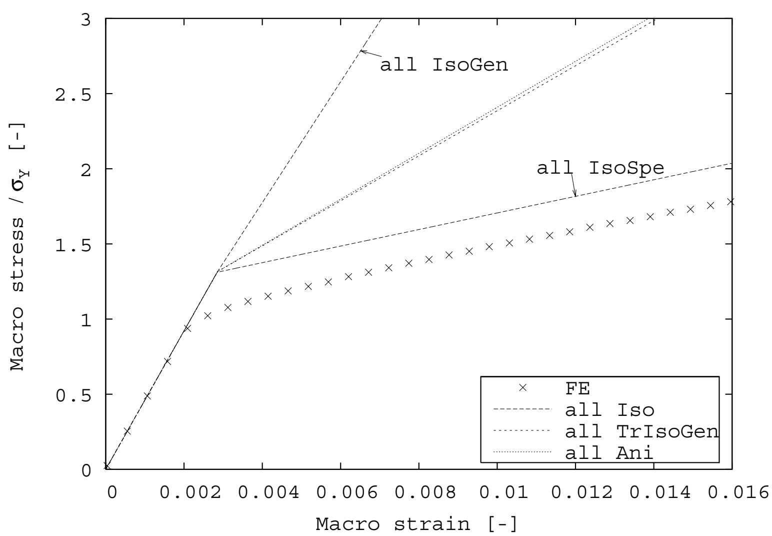

(b) Various computations of $\bar{\boldsymbol{C}}$.

Figure 5.4: Aluminum matrix with fibers. Longitudinal macroscopic tension test.

be corrected with the help of the softening coefficient so that predictions be-

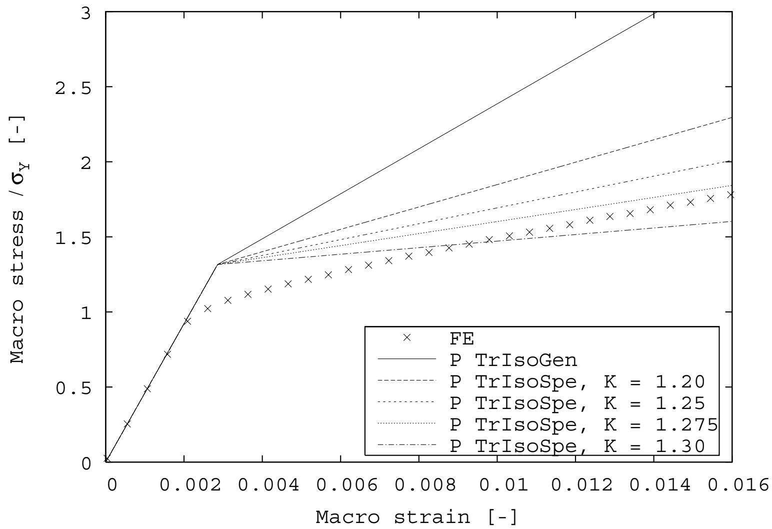

Figure 5.5: Aluminum matrix with fibers. Longitudinal macroscopic tension test. Various computations of $\boldsymbol{P}$ with the general and special transversely isotropic extraction method.

come much more realistic and can even give the best one among all the different computations.

5.4.2 Microscopic fields analysis

This section focuses on the accuracy of the microscopic fields and their influence on the macroscopic predictions. For this, three models are compared: first order secant formulation, second order secant formulation (results of these two models are provided by González and LLorca [81]) and the incremental formulation (obtained with DIGIMAT [23]). The latter always uses an isotropic extraction of the matrix modulus to compute the Eshelby's tensor only in order to soften the effective tangent operator (section 5.3). Throughout this section, the same composite is considered and consists of an elasto-plastic matrix ($E_m = 70$ GPa, $\nu_m = 0.33$, $\sigma_Y = 0$ MPa, hardening power law and $k = 400$ MPa) reinforced with ellipsoidal elastic inclusions ($E_i = 400$ GPa and $\nu_i = 0.20$) with small aspect ratio ($Ar = 3$). Two different values of the hardening exponent of the matrix are used: $n = 0.05$ and $n = 0.40$. Uniaxial traction tests are performed in both longitudinal and transverse directions. Such analysis enables to better evaluate homogenization schemes. Also, knowing the accuracy of the microscopic fields is a crucial issue since these govern damage initiation.

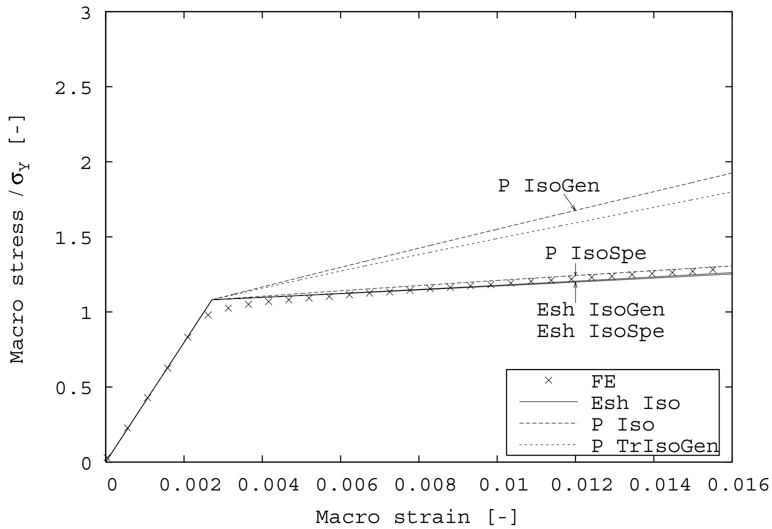

(a) Various computations of $\boldsymbol{P}$.

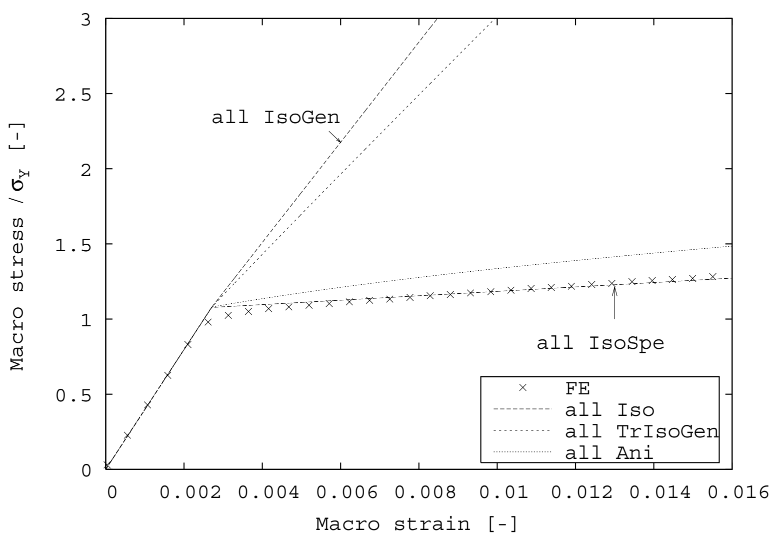

(b) Various computations of $\bar{\boldsymbol{C}}$.

Figure 5.6: Aluminum alloy with fibers. Transverse macroscopic tension test.

For validation purpose, predictions of mean-field homogenization schemes are confronted with FE simulations on 3D periodic unit cells (section 3.2).

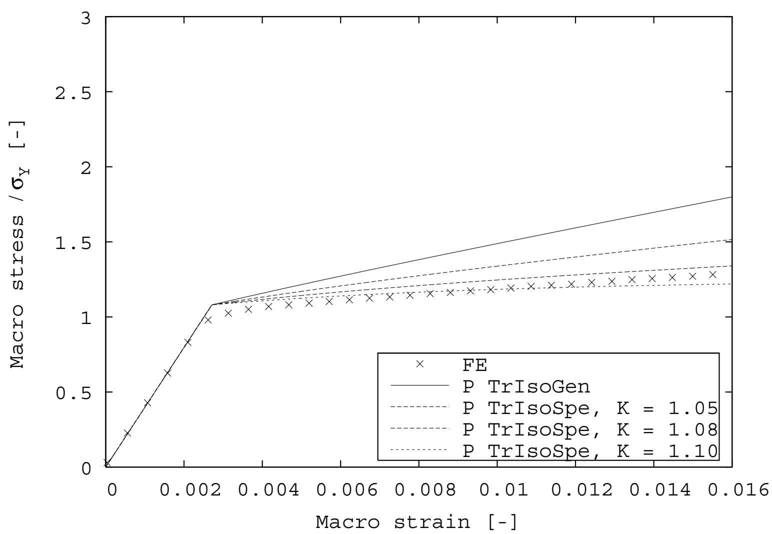

Figure 5.7: Aluminum alloy with fibers. Transverse macroscopic tension test. Various computations of $\boldsymbol{P}$ with the general and special transversely isotropic extraction method.

To check the accuracy of the FE simulations, four cells were generated and for each value of n, four traction tests were simulated in the longitudinal direction and eight in the transverse one. The scattering between these curves was generally very low, from a fraction of percent to a few percent. This being higher in the transverse direction and for $n = 0.05$. The quasi-exact reference prediction is obtained by averaging the four (or eight) curves.

Macroscopic results of mean-field homogenization and FE simulations are plotted on figures 5.10 and 5.11 for tension tests in both directions and for the two values of the hardening exponent. First-order secant method is generally the stiffest prediction while the second-order secant is the softest among the three homogenization schemes. The incremental formulation has intermediate predictions. It is interesting to notice that accuracy depends on the direction and the hardening. Differences being more pronounced for the longitudinal traction test and the low value of the hardening exponent. For the traction direction, this result was expected since curvature edges of the ellipsoids are higher in the longitudinal direction than the transverse one, where reinforcements behaves much more like spheres. This fact is illustrated on figure 5.12 where the accumulated plastic strain field is illustrated for both traction tests for a corresponding macro strain of 5% and $n = 0.05$. Heterogeneities are clearly

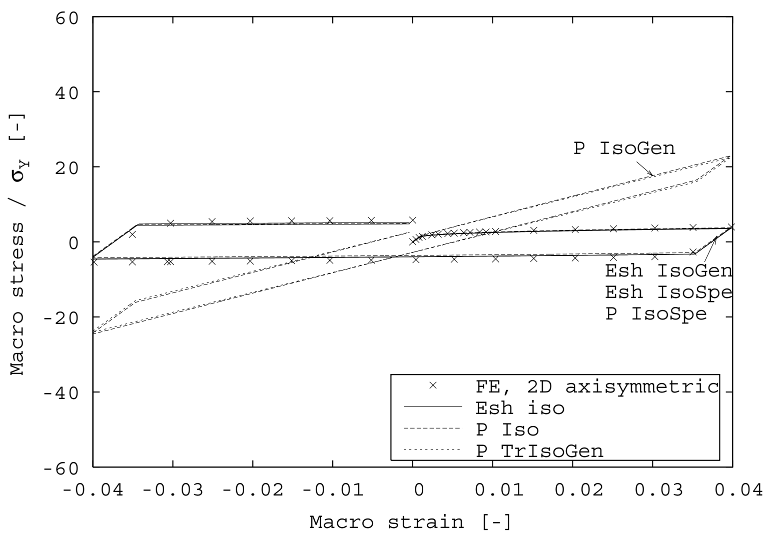

(a) Various computations of $\boldsymbol{P}$.

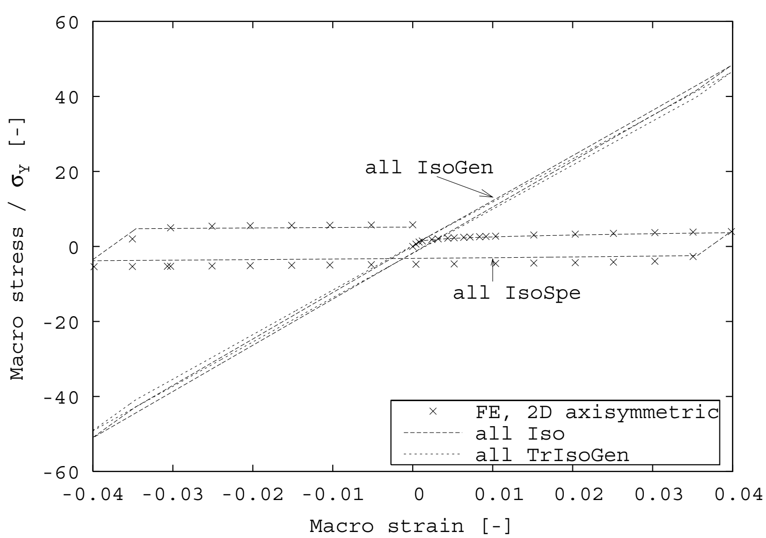

(b) Various computations of $\bar{\boldsymbol{C}}$.

Figure 5.8: MMC under cyclic strain.

more pronounced in the case of a longitudinal traction test. Furthermore, high levels of plasticity are found along the loading direction and especially between

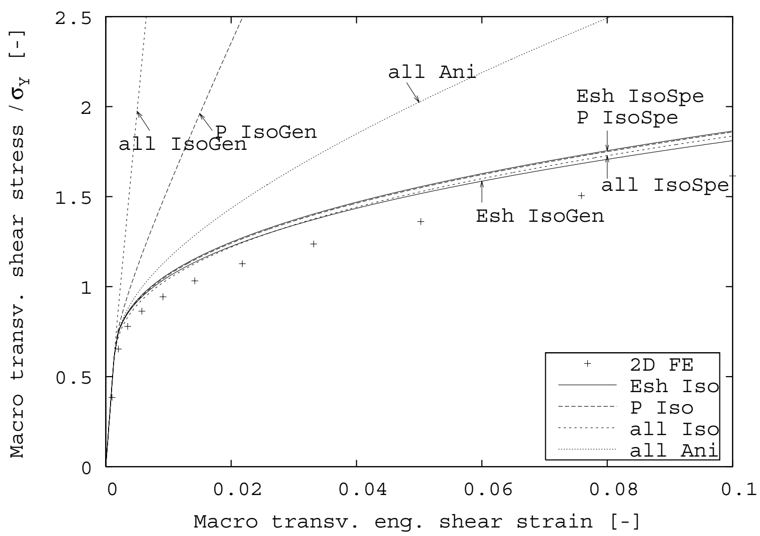

(a) Various computations of the macroscopic tangent operator.

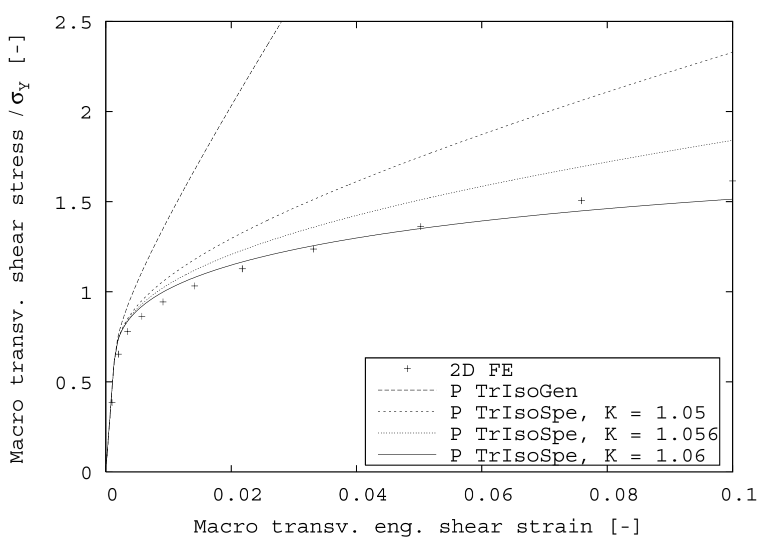

(b) Various computations of $\boldsymbol{P}$ with the general and special transversely isotropic extraction method.

Figure 5.9: MMC under transverse shear.

ellipsoids closely packed to each others. In order to measure the heterogeneity

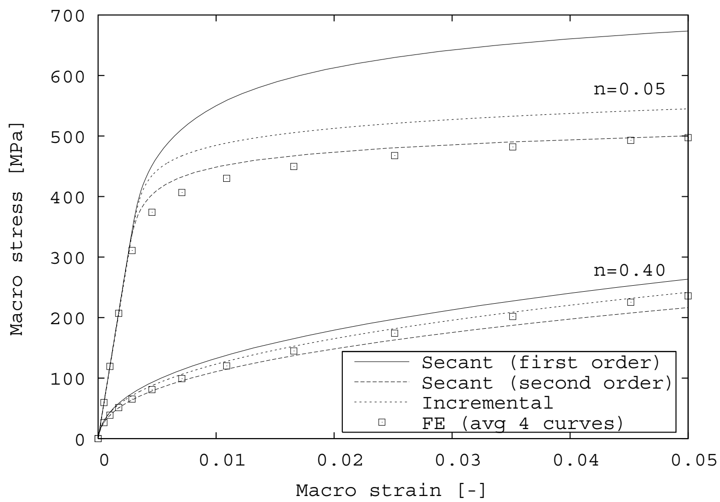

Figure 5.10: Predictions of the tensile stress-strain curves in the longitudinal direction for the composite reinforced with 25% of aligned ellipsoids.

of the accumulated plastic strain field, curves on figure 5.13 show the cumulative probability that the plastic strain is smaller than a given value. In order to compute it, magnitude of the plastic strain at each Gauss point of the matrix is considered as well as the corresponding volumes of these points. A perfectly homogeneous field would give a step function. The widest distribution is found for the longitudinal traction test and $n = 0.05$ while the field is much more homogeneous for the transverse traction test and a high value of the matrix hardening exponent. Such analysis is important in order to understand the behavior of homogenization schemes. Effectively, these rely on the definition of a per phase reference state (see section 5.2.1 for the secant formulation and section 5.2.2 for the incremental one) so that the average equivalent stress can be evaluated in an approximate way only. First order secant and incremental methods compute it from the per phase average stress tensor and this is known for being less accurate when high heterogeneity of the fields occur. The second order secant homogenization scheme relies on the second order moment of the stress tensor. However, all these values can be computed from the FE

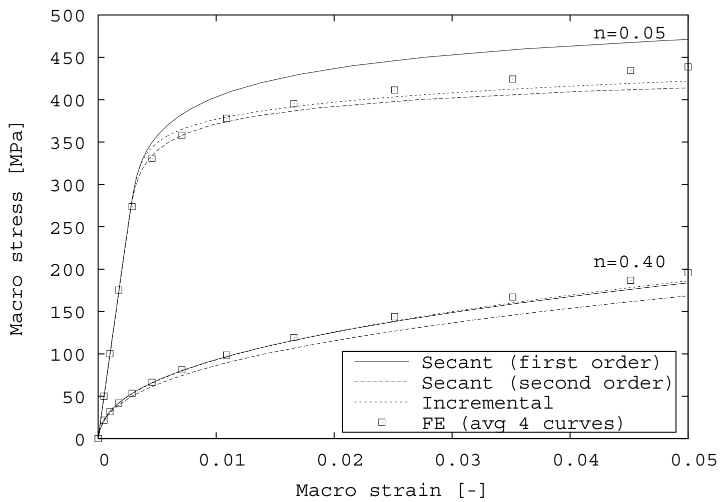

Figure 5.11: Predictions of the tensile stress-strain curves in the transverse direction for the composite reinforced with 25% of aligned ellipsoids.

simulations as (González *et al.* [37]):

$$< \sigma^{eq} >_{\omega_0} \quad = \quad \left[\sum_k \sigma_k^{eq} V_k \right] / \sum_k V_k, \tag{5.60}$$

$$< \boldsymbol{\sigma} >_{\omega_0} \quad = \quad \left[\sum_k \boldsymbol{\sigma}_k V_k \right] / \sum_k V_k, \tag{5.61}$$

$$< \boldsymbol{\sigma} \otimes \boldsymbol{\sigma} >_{\omega_0} \quad = \quad \left[\sum_k \left(\boldsymbol{\sigma}_k \otimes \boldsymbol{\sigma}_k \right) V_k \right] / \sum_k V_k, \tag{5.62}$$

where $\boldsymbol{\sigma}_k$ is the stress tensor at the Gauss point k and V_k is its corresponding volume. Equation (5.60) gives the average equivalent stress and equations (5.61-5.62) give first and second order moments. These enable to compute the reference equivalent stress used in the first order and second order secant methods (equations (5.7-5.8)). Average of the equivalent stress and the two reference values obtained by FE at a macroscopic deformation state of 5% are plotted on figure 5.14. Equivalent stresses computed from the second order moment of the stress tensor are extremely close to the reference result while the one computed from the average stress tensor is always lower. This fact being more pronounced for low hardening exponent and in the longitudinal direction. These lower reference equivalent stresses of the matrix for the first order secant approach lead

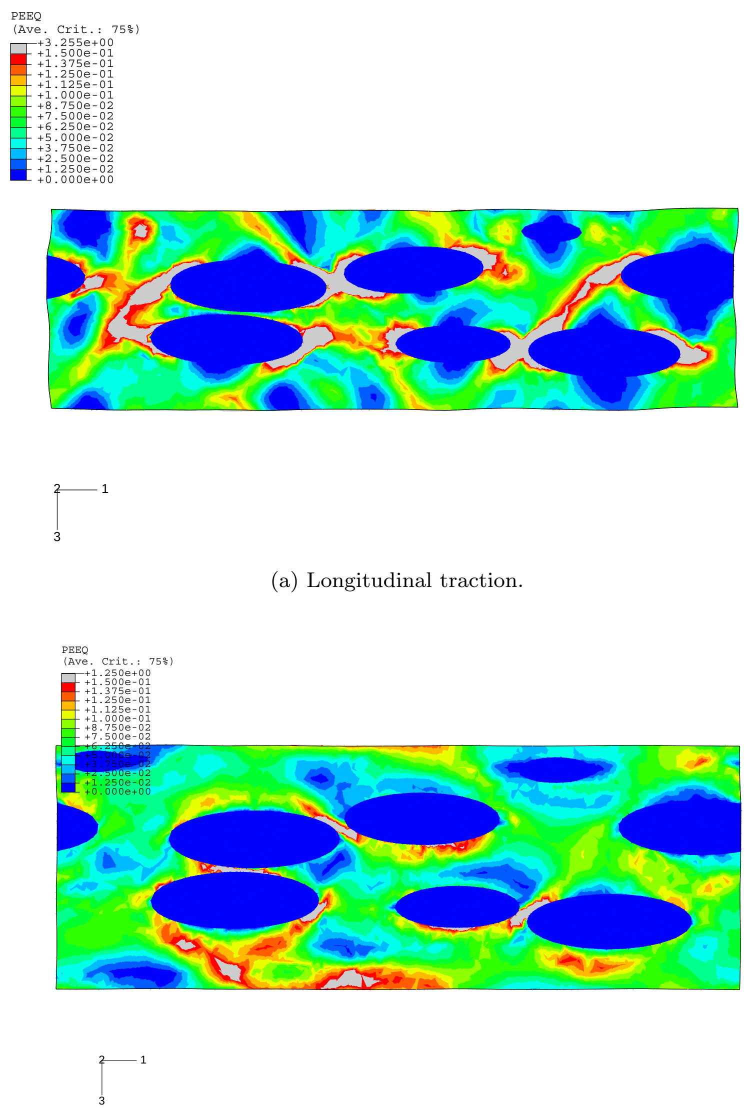

(a) Longitudinal traction.

(b) Transverse traction.

Figure 5.12: Contour plot of the accumulated plastic strain in the matrix after tensile deformation up to 5% in the composite with $n = 0.05$.

to much higher equivalent stresses in the inclusions than ones obtained by the second order method and finally give too stiff macroscopic predictions as shown

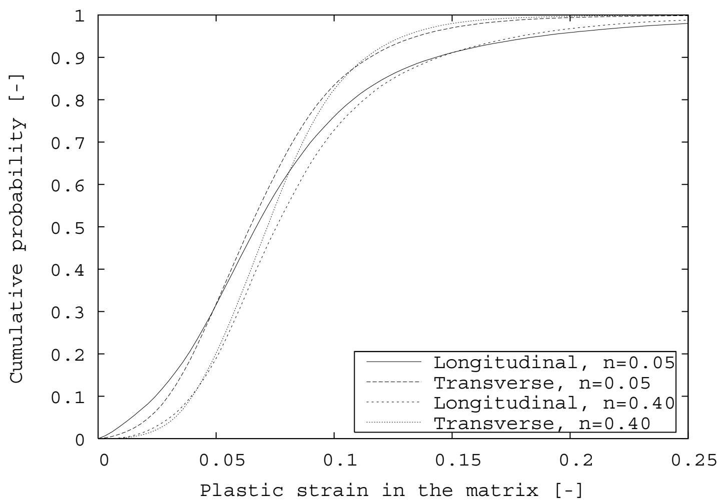

Figure 5.13: Cumulative probabilities of the plastic strain in the matrix as a function of the loading direction and of the matrix strain hardening exponent at a far-field applied strain of 5%.

on figures 5.10 and 5.11. After the study of the influence of the reference state on the macroscopic predictions, let's now examine the accuracy of the different homogenization schemes at the microscopic level. Effectively, even if a model provides a good estimation of the macroscopic behavior, this is not necessary true for the microscopic fields. This is illustrated on figure 5.15 for a traction test in the longitudinal direction and a high hardening exponent. Evolution of the matrix plastic strain is plotted with respect to the macroscopic strain (figure 5.15a). Plastic strain in the matrix is always underestimated by the mean-field homogenization schemes so that elastic effects dominate and the matrix hardening rate will be overestimated. This can be corrected either by using the second order secant method or the incremental one with a stiffness reduction of the matrix tangent operator. However, such approach decreases the accuracy of the von Mises equivalent stress in the inclusions (figure 5.15b), best prediction being then obtained with first order secant method. When looking at the components of the stress tensor in the phases, some surprises appear. For example, in the same simulation, the incremental method predicts a triaxial tension state in the inclusions and a compression in the direction of traction in the matrix even if the equivalent stress in both phases is not that far from the reference value. This illustrates the need for improvements in the per phase predictions of homogenization schemes, especially for modeling damage by either inclusions fracture or interface debonding. For such tests, FE simulations are, by far, the best predictive method. FE simulations to model damage modeling are given by LLorca and Segurado [64] and Segurado and LLorca [93].

5.5 Conclusions

In this chapter, various formulations of the local elasto-plastic constitutive laws were reviewed. The incremental formulation, which links over a time step the strain increment to the stress increment through a tangent operator has been studied in depth. For simplicity, we focused on the matrix phase, assumed that it obeys classical J_2 elasto-plasticity and considered the Mori-Tanaka homogenization scheme. A key issue in Eshelby-based nonlinear homogenization is to define a homogeneous tangent operator $\boldsymbol{C}_0(t)$ for a fictitious reference matrix. The tangent operator is anisotropic (and designated by $\boldsymbol{C}_0^{ani}$) and computing the overall tangent operator $\bar{\boldsymbol{C}}$ with $\boldsymbol{C}_0^{ani}$ leads to predictions which are too stiff and unacceptable. A known workaround is to compute the tensors of Eshelby ($\mathcal{E}$) or Hill ($\boldsymbol{P}$) with an isotropic part $\boldsymbol{C}_0^{iso}$ of $\boldsymbol{C}_0^{ani}$ and the rest of $\bar{\boldsymbol{C}}$ with $\boldsymbol{C}_0^{ani}$, but this method has been criticized as being unjustified or even wrong. Our opinion is that ideally $\bar{\boldsymbol{C}}$ should be computed with a given reference matrix tangent $\boldsymbol{C}_0$. The fact that $\boldsymbol{C}_0^{ani}$ leads to bad predictions means that it is a bad approximation to $\boldsymbol{C}_0$. In the absence of an appropriate expression for $\boldsymbol{C}_0$, the workaround consisting of computing part of $\bar{\boldsymbol{C}}$ (e.g. $\mathcal{E}$ or $\boldsymbol{P}$) with $\boldsymbol{C}_0^{iso}$ and the rest with $\boldsymbol{C}_0^{ani}$ is acceptable as long as it leads to good predictions and is no less legitimate than computing all of $\bar{\boldsymbol{C}}$ with $\boldsymbol{C}_0^{ani}$. In this work, we chose to examine different variants for the computation of $\bar{\boldsymbol{C}}$ and understand why some work better than others by studying some of their mathematical properties. Some key points are recalled and discussed hereafter.

Hill's tensor ($\boldsymbol{P}$) and the overall tangent ($\bar{\boldsymbol{C}}$) are decreasing and increasing functions of $\boldsymbol{C}_0$, respectively:

$$\boldsymbol{P}(\boldsymbol{C}_0 + \Delta\boldsymbol{C}) < \boldsymbol{P}(\boldsymbol{C}_0), \;\; \bar{\boldsymbol{C}}(\boldsymbol{C}_0 + \Delta\boldsymbol{C}) > \bar{\boldsymbol{C}}(\boldsymbol{C}_0), \;\; \Delta\boldsymbol{C} > 0. \tag{5.63}$$

A similar result for $\bar{\boldsymbol{C}}$ holds when only the argument of $\boldsymbol{P}$ is changing:

$$\bar{\boldsymbol{C}}(\boldsymbol{P}(\boldsymbol{C}_0 + \Delta\boldsymbol{C}), \boldsymbol{C}_0) > \bar{\boldsymbol{C}}(\boldsymbol{P}(\boldsymbol{C}_0), \boldsymbol{C}_0), \;\; \Delta\boldsymbol{C} > 0. \tag{5.64}$$

Two isotropic extractions of $\boldsymbol{C}_0^{ani}$ exist: a general projection method (giving $\boldsymbol{C}_0^{IsoGen}$) and a special method ($\boldsymbol{C}_0^{IsoSpe}$). The following relations hold:

$$\boldsymbol{C} > \boldsymbol{C}_0^{ani} \geq \boldsymbol{C}_0^{IsoSpe}. \tag{5.65}$$

Therefore $\bar{\boldsymbol{C}}$ computed with the isotropic operator $\boldsymbol{C}_0^{IsoSpe}$ is softer than the one computed with anisotropic operators $\boldsymbol{C}_0^{ani}$, i.e.

$$\bar{\boldsymbol{C}}(\boldsymbol{C}_0^{IsoSpe}) < \bar{\boldsymbol{C}}(\boldsymbol{C}_0^{ani}), \;\; \bar{\boldsymbol{C}}(\boldsymbol{P}(\boldsymbol{C}_0^{IsoSpe}), \boldsymbol{C}_0) < \bar{\boldsymbol{C}}(\boldsymbol{P}(\boldsymbol{C}_0^{ani}), \boldsymbol{C}_0). \tag{5.66}$$

However, we found that in some cases (e.g., macro tension) the following result holds:

$$\boldsymbol{C}_0^{IsoGen} > \boldsymbol{C}_0^{ani}, \tag{5.67}$$

which means that the isotropic operator $\boldsymbol{C}_0^{IsoGen}$ is stiffer than the anisotropic one, and this implies that:

$$\bar{\boldsymbol{C}}(\boldsymbol{C}_0^{IsoGen}) > \bar{\boldsymbol{C}}(\boldsymbol{C}_0^{ani}), \;\; \bar{\boldsymbol{C}}(\boldsymbol{P}(\boldsymbol{C}_0^{IsoGen}), \boldsymbol{C}_0) > \bar{\boldsymbol{C}}(\boldsymbol{P}(\boldsymbol{C}_0^{ani}), \boldsymbol{C}_0). \tag{5.68}$$

This surprising and unexpected result may be interpreted physically following Chaboche *et al.* [18], [19]. Indeed, the special method (at least under proportional loading) corresponds to a stiffness reduction of $\boldsymbol{C}_0^{ani}$ in a direction orthogonal to that of the reference flow direction ($\boldsymbol{N}$). Moreover the stiffness reduction effect is much more important with the special method than with the general one.

In this chapter, we also extracted transversely isotropic parts of $\boldsymbol{C}_0^{ani}$ using a general projection method (giving $\boldsymbol{C}_0^{TrIsoGen}$) or a special one ($\boldsymbol{C}_0^{TrIsoSpe}$). In summary, in addition to $\boldsymbol{C}_0^{ani}$, we considered two isotropic projections ($\boldsymbol{C}_0^{IsoGen}$ and $\boldsymbol{C}_0^{IsoSpe}$) and two transversely isotropic ones ($\boldsymbol{C}_0^{TrIsoGen}$ and $\boldsymbol{C}_0^{TrIsoSpe}$). Designating anyone of these five operators by $\boldsymbol{C}_0$, $\boldsymbol{D}_0$ or $\boldsymbol{E}_0$, we studied different variants of the incremental formulation by computing Hill's tensor as:

$$\boldsymbol{P} = \mathcal{E}(\boldsymbol{E}_0) : \boldsymbol{D}_0^{-1} \tag{5.69}$$

and the rest of $\bar{\boldsymbol{C}}$ with $\boldsymbol{C}_0$. We conducted a series of validated numerical simulations for a variety of composites with different types of inclusions (long or short fibers, spherical particles) under various loads (longitudinal or transverse tension, transverse shear). The main conclusions are listed hereafter.

The sets which work best in most cases are the following:

$$\boldsymbol{E}_0 = \boldsymbol{C}_0^{IsoGen} \text{ or } \boldsymbol{C}_0^{IsoSpe}, \quad \boldsymbol{D}_0 = \boldsymbol{C}_0 = \boldsymbol{C}_0^{ani}. \tag{5.70}$$

In some cases, they fail and give physically unacceptable results, which is especially noticeable for materials reinforced with long fibers. This corresponds to $\boldsymbol{P}$ losing diagonal (major) symmetry. When this happens, the following set gives good results:

$$\boldsymbol{E}_0 = \boldsymbol{D}_0 = \boldsymbol{C}_0^{IsoSpe}, \text{ i.e. } \boldsymbol{P}(\boldsymbol{C}_0^{IsoSpe}), \, \boldsymbol{C}_0 = \boldsymbol{C}_0^{ani}. \tag{5.71}$$

It also leads to good predictions in most cases. However the choice $\boldsymbol{P}(\boldsymbol{C}_0^{IsoGen})$ leads to bad (too stiff) predictions. Another set which works in many cases is the following:

$$\boldsymbol{E}_0 = \boldsymbol{D}_0 = \boldsymbol{C}_0 = \boldsymbol{C}_0^{IsoSpe}, \text{ i.e. } \boldsymbol{P}(\boldsymbol{C}_0^{IsoSpe}) \text{ and } \bar{\boldsymbol{C}}(\boldsymbol{C}_0^{IsoSpe}). \tag{5.72}$$

Unfortunately, the use of $\boldsymbol{C}_0^{IsoSpe}$ is limited to constitutive models for which the anisotropic tangent operator can be cast under the particular form (5.29).

If this is not the case and if the use of $\boldsymbol{C}_0^{IsoGen}$ in (5.70) gives bad results, we advice to use the special method of the transversely isotropic projection with the following set:

$$\boldsymbol{E}_0 = \boldsymbol{D}_0 = \boldsymbol{C}_0^{TrIsoSpe}, \text{ i.e. } \boldsymbol{P}(\boldsymbol{C}_0^{TrIsoSpe}), \quad \boldsymbol{C}_0 = \boldsymbol{C}_0^{ani}. \tag{5.73}$$

The case $\boldsymbol{P}(\boldsymbol{C}_0^{TrIsoGen})$ gives extremely stiff predictions. This means that $\boldsymbol{C}_0^{TrIsoGen}$ is too stiff. Similarly to isotropic projections, this might be explained by the fact that the general transversely isotropic projection is a mathematical definition with no physical basis. Other sets studied, namely $\bar{\boldsymbol{C}}(\boldsymbol{C}_0^{IsoGen})$, $\bar{\boldsymbol{C}}(\boldsymbol{C}_0^{TrIsoGen})$ and $\bar{\boldsymbol{C}}(\boldsymbol{C}_0^{ani})$ all lead in general to unacceptably stiff predictions.

In the future, one could improve some points. For instance, in the transversely isotropic projection, try an anisotropy direction other than the ellipsoids' revolution axis or find a better special stiffness reduction method with no arbitrary coefficient K. Real progress in Eshelby-based nonlinear homogenization is possible only with new approaches in computing reference matrix tangent operator $\boldsymbol{C}_0(t)$, for instance with phase-averaged second-order moments of stress or strain. However, extending the latter approach to an incremental formulation and to sophisticated micro constitutive models remains an open question.

In order to analyze the influence of the per phase reference state and compare different formulations of the constitutive laws, the first order incremental formulation was confronted to both first and second order secant formulations and to FE simulations. The considered composite for this analysis was made of a matrix reinforced by 25% of aligned and randomly distributed ellipsoidal inclusions (Ar=3) and the Mori-Tanaka homogenization scheme was used. Different matrix strain hardening were considered and uniaxial traction tests were performed in both longitudinal and transverse directions.

For the overall predictions, best ones were obtained by the incremental and the second order secant formulations while the first order secant method gave generally too stiff results. The incremental tended to overestimate the composite flow stress when the localization of the plastic strain in the matrix was maximum, which occurred for the longitudinal tension test and a low matrix hardening exponent. Comparison of the volumetric-average fields in each phase showed that accurate predictions of the effective properties by the homogenization methods did not guarantee the same accuracy at the phase level.

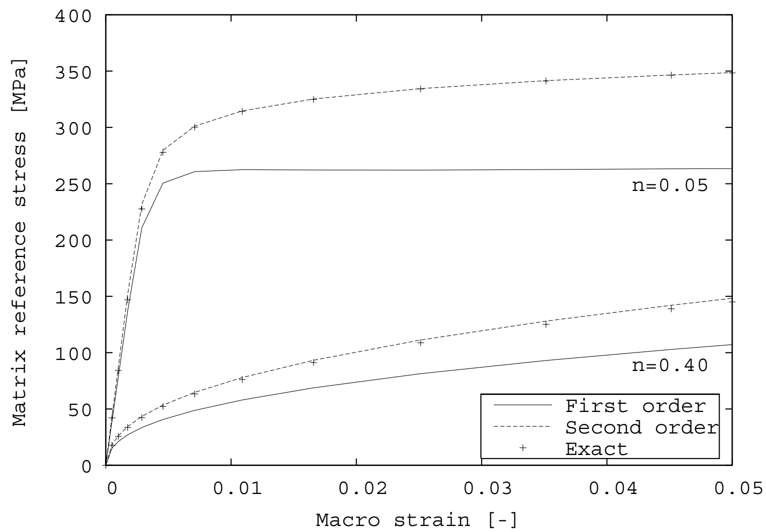

(a) Longitudinal deformation.

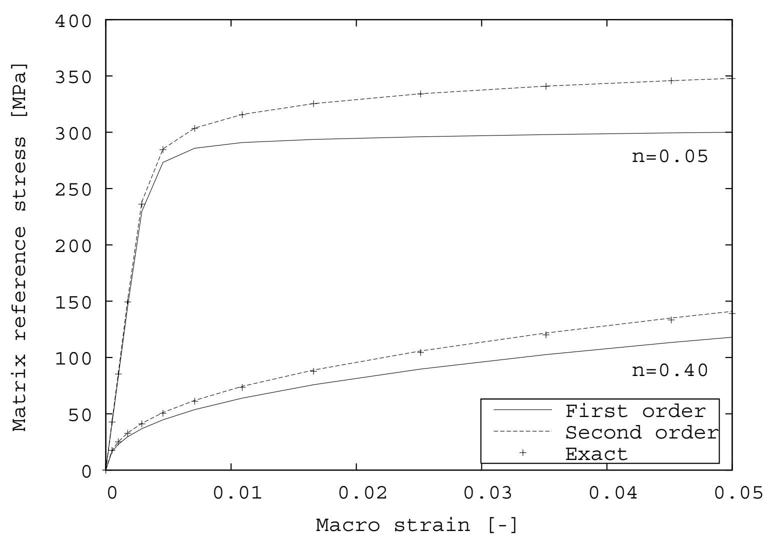

(b) Transverse deformation.

Figure 5.14: Evolution of the actual volume-averaged reference stress in the matrix ($\bar{\sigma}_m^{eq}$) as a function of the applied strain and of the estimation based on the volume-averaged first ($\hat{\sigma}_m^{eq}$) and second-order ($\hat{\hat{\sigma}}_m^{eq}$) moment of the matrix stress tensor.

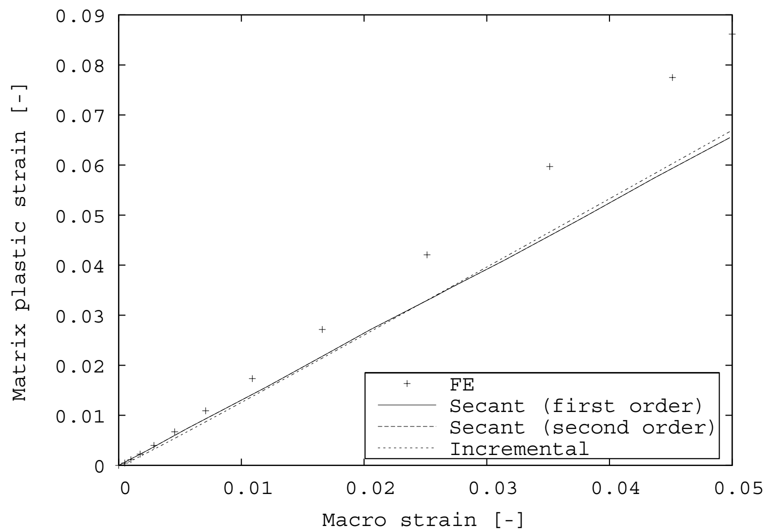

(a) Evolution of the plastic strain the matrix as a function of the applied strain.

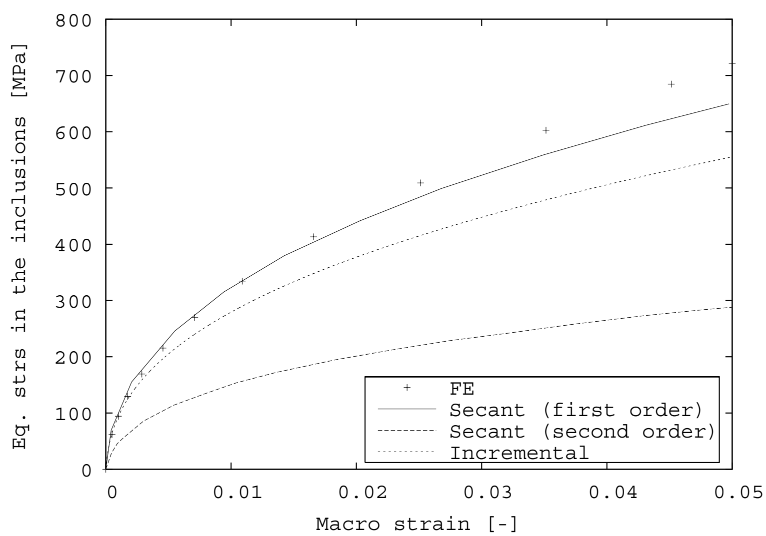

(b) Evolution of the von Mises equivalent stress in the ellipsoids as a function of the applied strain.

Figure 5.15: The composite is loaded in the longitudinal direction (matrix strain hardening exponent is 0.40).